Results

Patient characteristics

Of the 51 exudative AMD patients, 31 patients (61%) were diagnosed with tAMD, and the remaining 20 patients (39%) were diagnosed with PCV. The baseline characteristics of study participants are summarized in Table 1. At baseline, the distribution of age, gender, great linear dimension (GLD), logMAR vision and central retinal thickness were not significantly different between tAMD and PCV ($P > 0.05$) patients. However, patients with tAMD had classic lesions more frequently than patients with PCV ($P = 7.81 \times 10^{-4}$).

Visual outcomes

The mean logMAR vision in all AMD patients was 0.807 (corresponding approximate VA score: 0.15) at the baseline examination and 0.937 (corresponding approximate visual acuity score: 0.11) at the month 60 examination. The logMAR vision gradually decreased throughout the follow-up period, but the difference between baseline and month 60 was not significant in each subset group (tAMD; $P = 0.110$, PCV; $P = 0.290$, all AMD; $P = 0.052$) (Figure 1).

Mean logMAR vision loss was similar between patients with tAMD and with PCV. The significant difference was not demonstrated in the change of logMAR vision from baseline between tAMD and PCV throughout the follow-up period ($P = 0.814$ at month 6, 0.957 at month 12, 0.544 at month 24 and 0.781 at month 60). LogMAR vision of patients with occult CNV improved from 0.822 ± 0.419 at baseline to 0.781 ± 0.516 at month 24 while logMAR vision of patients with classic CNV worsened from 0.796 ± 0.311 at baseline to 0.884 ± 0.473 at month 24. However, the significant difference was not seen between these patient groups throughout the follow up ($P = 0.097$ at month 6, $P = 0.518$ at month 12, $P = 0.595$ at month 24 and $P = 0.197$ at month 60).

Figure 2 demonstrates mean change in letters from baseline (logMAR vision converted to visual acuity letter scores) throughout 60-month follow up for all patients with AMD, tAMD and PCV (Figure 2A) and for 30 patients with classic CNV and 21 patients with occult CNV (Figure 2B). Mean visual acuity letter score decreased 6.51 in patients with all AMD, 7.25 in patients with tAMD and 5.36 in patients with PCV at the month 60 examination (Figure 2A). The patients with lesions of predominantly or minimally classic CNV had 10.0 letters loss, but the patients with lesions of occult with no classic CNV had only 1.43 letters loss (Figure 2B).

Number of retreatments

The mean number of retreatments per year during the follow up period is shown in Table 2. The number of retreatments peaked in year 1 and declined along the time course for patients with tAMD, but patients with PCV had significantly more frequent retreatments in the years 3 and 4 than patients with tAMD ($P = 1.48 \times 10^{-2}$, 5.96×10^{-3}, respectively).

Discussion

A previous randomized clinical trial for Japanese AMD (JAT study) provided 1-year results of PDT, demonstrating better angiographic and vision effects to those observed in Caucasian patients.[4] JAT extension study showed similar favorable results through 2-year follow up. Mean visual acuity letter score in the study eye increased from 50.8 at baseline to 54.0 at month 24. In contrast to those reports, the mean logMAR vision in all AMD patients decreased from 0.807 (corresponding approximate visual acuity score: 0.15) at the baseline to 0.937 (corresponding approximate visual acuity score: 0.11) at the month 60 examination. Although many previous reports, with up to 12 months follow up results, described favorable results of PDT in treating PCV,[19–23] our data did not show the significant

Table 1 Baseline characteristics of study participants

	tAMD	PCV	P
Number of patients	31	20	
Age (mean ± SD)	70.3 ± 7.2	69.5 ± 7.5	0.686*
Sex (male/female)	24/7	16/4	0.826†
Angiographic classification (classic/occult)‡	24/7	6/14	7.81×10^{-4}†
GLD (μm, mean ± SD)	3172 ± 1352	3550 ± 1321	0.834*
Mean BCVA, logMAR vision (mean ± SD)	0.85 ± 0.33	0.73 ± 0.40	0.141*
Mean BCVA, corresponding approximate decimal visual acuity	0.141	0.186	
Mean CRT (μm, mean ± SD)	489 ± 143	541 ± 195	0.815*

Notes: *Unpaired t-test; †Chi-square test; ‡fluorescein angiographic classification, classic indicates patients with lesions composed of predominantly or minimally classic CNV and occult indicates patients with lesions composed of occult with no classic choroidal neovascularization (CNV).

Abbreviations: tAMD, typical neovascular age-related macular degeneration; PCV, polypoidal choroidal vasculopathy; SD, standard deviation; GLD, greatest linear dimension; BCVA, best corrected visual acuity; logMAR, logarithm of minimum angular resolution; CRT, central retinal thickness.

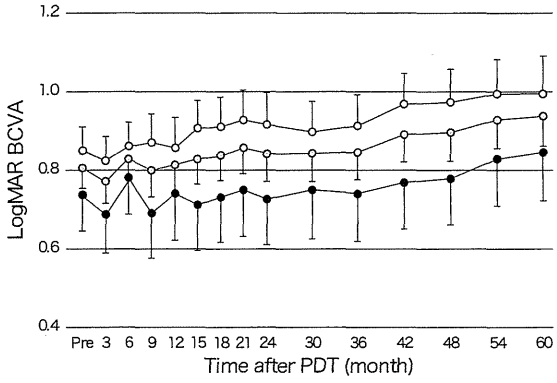

Figure 1 Best corrected visual acuity (BCVA) for all neovascular age-related macular degeneration (AMD), typical neovascular AMD (tAMD) and polypoidal choroidal vasculopathy (PCV) patients after photodynamic therapy (PDT) (open circles, tAMD; gray circles, all AMD; solid circles, PCV) over the 60 month follow-up period.
Notes: The BCVA was determined using the Landolt C chart, and was calculated and presented as the logarithm of the minimum angle of resolution (logMAR). Values are presented as mean. (Error bar and standard error).
Abbreviation: PDT, photodynamic therapy.

difference in visual prognosis between tAMD and PCV after long-term follow-up. Mean visual acuity letter score loss is similar between patients with tAMD and with PCV at the month 60 examination with no significant difference. These facts suggest that the better results in Japanese AMD patients and predominance of PCV in the visual outcome may be temporal during the first 2 years and may not last for more than 5 years.

Interestingly, this study demonstrated that the patients with lesions of classic CNV had 10.0 letters loss, while the patients with lesions of occult CNV had only 1.43 letters loss in 5 years. Patients with occult CNV gained 5.81 letters at month 6 and 2.07 at month 24 while patients with classic CNV lost 5.96 letters at month 6 and 4.39 at month 24. However, the significant difference was not seen between these a patient groups throughout the follow up. Figure 3 provides a comparative summary of visual outcomes of our study and the TAP investigation.[2,5,25] There were smaller proportions of patients who had at least a 15-letter loss in patients with occult CNV when compared to those with classic CNV.

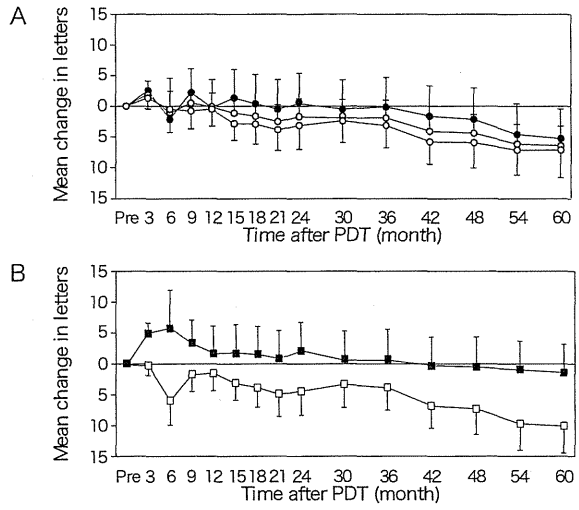

Figure 2 Mean change in letters from baseline for all long-term verteporfin treated patients; (**A**) open circles, tAMD; gray circles, all AMD; solid circles, PCV, (**B**) open squares, the patients with classic CNV; solid squares, the patients with occult CNV.
Note: (Error bar and standard error).
Abbreviation: PDT, photodynamic therapy; tAMD, typical neovascular; AMD, age-related macular degeneration; PCV, polypoidal choroidal vasculopathy; CNV, choroidal neonvascularization.

Table 2 Mean number of retreatments

	Number of retreatments during each yearly period (mean ± SD)		
	tAMD	PCV	P
Year 1	0.55 ± 0.72	0.35 ± 0.48	0.286
Year 2	0.16 ± 0.37	0.25 ± 0.44	0.446
Year 3	0.10 ± 0.30	0.45 ± 0.68	1.48×10^{-2}*
Year 4	0.03 ± 0.18	0.30 ± 0.47	5.96×10^{-3}*
Year 5	0.03 ± 0.18	0.10 ± 0.31	0.325

Note: *Significant (unpaired t-test).
Abbreviations: AMD, age-related macular degeneration; tAMD, typical neovascular AMD; PCV, polypoidal choroidal vasculopathy; SD, standard deviation.

The number of retreatments peaked in year 1 and declined along the time course for patients with tAMD, but patients with PCV had significantly more frequent retreatments in the years 3 and 4 than patients with tAMD ($P = 1.48 \times 10^{-2}$, $P = 5.96 \times 10^{-3}$, respectively). Honda et al also described 30-month results of PDT for Japanese patients with tAMD and PCV.[26] They found that recurrence of lesions in the PCV patients was more frequent than of that with the tAMD patients during the12–30 months after initial PDT, while the recurrence rate was lower in the PCV group during the first 12 months. Our finding is consistent to this report. The higher incidence of recurrence in PCV patients in the years 3 and 4 may explain

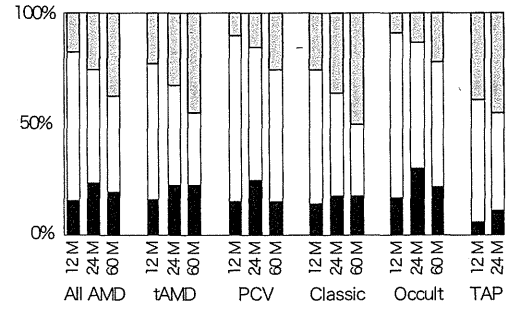

Figure 3 Comparison of visual outcomes for all patients at month 12, 24 and 60 with those of Treatment of Age-related Macular Degeneration with Photodynamic Therapy (TAP) Investigation.[2,5,25]
Notes: Black bars: ≥15-letters increase; white bars: no change (±14 letters); gray bars: ≥15-letters decrease.
Abbreviations: AMD, age-related macular degeneration; tAMD, typical age-related macular degeneration; PCV, polypoidal choroidal vasculopathy; TAP, treatment of age-related macular degeneration with photodynamic therapy study.

predominance of PCV in the visual outcome is temporal during the initial 2 years and does not last for more than 5 years.

There are at least two limitations to this study. One is the small sample size, which may be associated with low statistical power, which may or may not be a reason of no significant change in VA from baseline or no significant difference in VA between tAMD and PCV detected at any time point over 5-years of follow-up. The second is that the retrospective nature of the study might exclude the patients with excellent or bad courses that could cause bias in the results. Since several antivascular endothelial growth factor drugs other than PDT are currently available and have become the first-choice treatment for AMD, it might be difficult to overcome these limitations with a single report. However, meta-analysis with an accumulation of similar data with multiple publications may be one alternative measure for these limitations, and is warranted.

Acknowledgement

This research was supported in part by an Institutional Grant (20-1-2-02) from the Medical Research Center, Saitama Medical University (KM), a grant from the Eye Research Foundation for the Aged (KM) and a grant-in-aid for scientific research (21592242) from the Ministry of Education, Culture and Science in Japan (KM).

The sponsor or funding organization had no role in the design or conduct of this research.

Disclosure

The authors report no conflicts of interest in this work.

References

1. Vingerling LR, Diclemans IJ, Hofman A, et al. The prevalence of age related maculopathy in Rotterdam study. *Ophthalmology*. 1995;102:205–210.
2. Treatment of age-related macular degeneration with photodynamic therapy (TAP) Study Group. Photodynamic therapy of subfoveal choroidal neovascularization in age-related macular degeneration with verteporfin: one-year results of 2 randomized clinical trials-TAP report. *Arch Ophthalmol*. 1999;117:1329–1345.
3. Verteporfin in Photodynamic Therapy (VIP) Study Group. Verteporfin therapy of subfoveal choroidal neovascularization in age-related macular degeneration: two-year results of a randomized clinical trial including lesions with occult with no classic choroidal neovascularization-verteporfin in photodynamic therapy report 2. *Am J Ophthalmol*. 2001;131:541–560.
4. Japanese Age-Related Macular Degeneration Trials (JAT) Study Group. Japanese age-related macular degeneration trial: 1-year results of photodynamic therapy with verteporfin in Japanese patients with subfoveal choroidal neovascularization secondary to age-related macular degeneration. *Am J Ophthalmol*. 2003;135:1049–1061.
5. Treatment of age-related macular degeneration with photodynamic therapy (TAP) Study Group. Photodynamic therapy of subfoveal choroidal neovascularization in age-related macular degeneration with verteporfin: two-year results of 2 randomized clinical trials-TAP report 2. *Arch Ophthalmol*. 2001;119:198–207.
6. Verteporfin in Photodynamic Therapy Study Group. Photodynamic therapy of subfoveal choroidal neovascularization in pathologic myopia with verteporfin. 1-year results of a randomized clinical trial-VIP report no 1. *Ophthalmology*. 2001;108:841–852.
7. Blinder KJ, Bradley S, Bressler NM, et al. Treatment of Age-related Macular Degeneration with Photodynamic Therapy study group; Verteporfin in Photodynamic Therapy study group. Effect of lesion size, visual acuity, and lesion composition on visual acuity change with and without verteporfin therapy for choroidal neovascularization secondary to age-related macular degeneration: TAP and VIP report no 1. *Am J Ophthalmol*. 2003;136:407–418.
8. Barbazetto I, Burdan A, Bressler NM, et al. Treatment of Age-Related Macular Degeneration with Photodynamic Therapy Study Group; Verteporfin in Photodynamic Therapy Study Group. Photodynamic therapy of subfoveal choroidal neovascularization with verteporfin: fluorescein angiographic guidelines for evaluation and treatment-TAP and VIP report no 2. *Arch Ophthalmol*. 2003;121:1253–1268.
9. Arnold JI, Blinder KJ, Bressler NM, et al. Treatment of Age-related Macular Degeneration with Photodynamic Therapy study group; Verteporfin in Photodynamic Therapy study group. Acute severe visual acuity decrease after photodynamic therapy with verteporfin: case reports from randomized clinical trials-TAP and VIP report no 3. *Am J Ophthalmol*. 2004;137:683–696.
10. Bird AC, Bressler NM, Bressler SB, et al. An international classification and grading system for age-related macular degeneration. The International ARM Epidemiological Study Group. *Surv Ophthalmol*. 1995;39:367–374.
11. Spaide RF, Yannuzzi LA, Slakter JS, Sorenson J, Orlach DA. Indocyanine green videoangiography of idiopathic polypoidal choroidal vasculopathy. *Retina*. 1995;15:100–110.
12. Yannuzzi LA, Ciardella A, Spaide RF, Rabb M, Freund KB, Orlock DA. The expanding clinical spectrum of idiopathic polypoidal choroidal vasculopathy. *Arch Ophthalmol*. 1997;115:478–485.
13. Yannuzzi LA, Wong DWK, Storzolini BS, et al. Polypoidal choroidal vasculopathy and neovascularized age-related macular degeneration. *Arch Ophthalmol*. 1999;117:1503–1510.
14. Ciardella AP, Donsoff IM, Huang SJ, Costa DL, Yannuzzi LA. Polypoidal choroidal vasculopathy. *Surv Ophthalmol*. 2004;49:25–37.
15. Sho K, Takahashi K, Yamada H, et al. Polypoidal choroidal vasculopathy: incidence, demographic features, and clinical characteristics. *Arch Ophthalmol*. 2003;121:1392–1396.
16. Yuzawa M, Mori R, Kawamura A. The origins of polypoidal choroidal vasculopathy. *Br J Ophthalmol*. 2005;89:602–607.
17. Maruko I, Iida T, Ssito M, Nagayama D, Saito K. Clinical characteristics of exudative age-related macular degeneration in Japanese patients. *Am J Ophthalmol*. 2005;144:15–22.
18. Mori K, Horie-inoue K, Gerhlbach PL, et al. Phenotype and genotype characteristics of age-related macular degeneration in Japanese population. *Ophthalmology*. 2010;117:928–938.
19. Spaide RF, Donsoff I, Lam DL, et al. Treatment of polypoidal choroidal vasculopathy with photodynamic therapy. *Retina*. 2002;22:529–535.
20. Quaranta M, Maget-Faysse M, Coscas G. Exudative idiopathic polypoidal choroidal vasculopathy and photodynamic therapy with verteporfin. *Am J Ophthalmol*. 2002;134:277–280.
21. Chan WM, Lam DS, Lai TY, et al. Photodynamic therapy with verteporfin for symptomatic polypoidal choroidal vasculopathy. One-year results of a prospective case series. *Ophthalmology*. 2004;111:1576–1584.
22. Lee SC, Seong YS, Kim SS, Koh HJ, Kwon OW. Photodynamic therapy with verteporfin for polypoidal choroidal vasculopathy of the macula. *Ophthalmologica*. 2004;218:193–201.
23. Silva Rm, Figueira J, Cachulo ML, Duarte L, Faria de Abreu JR, Cunha-Vaz JG. Polypoidal choroidal vasculopathy and photodynamic therapy with verteporfin. *Graefes Arch Clin Exp Ophthalmol*. 2005;243:973–979.

24. Japanese Age-Related Macular Degeneration Trials (JAT) Study Group. Photodynamic therapy with verteporfin in Japanese patients with subfoveal choroidal neovascularization secondary to age-related macular degeneration (AMD): results of the Japanese AMD Trial (JAT) extension. *Jpn J Ophthalmol.* 2008;52:99–107.
25. Treatment of Age-Related Macular Degeneration with Photodynamic therapy (TAP) Study Group. Verteporfin therapy for subfoveal choroidal neovascularization in age-related macular degeneration: 5-year results of an open-label extension of 2 randomized clinical trials-TAP report no 8. *Graefes Arch Clin Exp Ophthalmol.* 2006;244:1132–1142.
26. Honda S, Kurimoto Y, Kagotani Y, Yamamoto H, Takagi H, Uenishi M. Hyogo Macular Disease Study Group. Photodynamic therapy for typical age-related macular degeneration and polypoidal choroidal vasculopathy: a 30-month multicenter study in Hyogo, Japan. *Jpn J Ophthalmol.* 2009;53:593–597.

HMG Advance Access published May 21, 2013

Human Molecular Genetics, 2013 **1–9**
doi:10.1093/hmg/ddt210

Enhanced optineurin E50K–TBK1 interaction evokes protein insolubility and initiates familial primary open-angle glaucoma

Yuriko Minegishi[1], Daisuke Iejima[1], Hiroaki Kobayashi[1], Zai-Long Chi[1], Kazuhide Kawase[2], Tetsuya Yamamoto[2], Tomohisa Seki[3], Shinsuke Yuasa[3], Keiichi Fukuda[3] and Takeshi Iwata[1,*]

[1]Division of Molecular and Cellular Biology, National Institute of Sensory Organs, National Hospital Organization Tokyo Medical Center, Tokyo, Japan [2]Department of Ophthalmology, Gifu University School of Medicine, Gifu, Japan [3]Department of Cardiology, Keio University School of Medicine, Tokyo, Japan

Received March 13, 2013; Revised April 15, 2013; Accepted May 1, 2013

Glaucoma is the leading cause for blindness affecting 60 million people worldwide. The optineurin (OPTN) E50K mutation was first identified in familial primary open-angle glaucoma (POAG), the onset of which is not associated with intraocular pressure (IOP) elevation, and is classified as normal-tension glaucoma (NTG). Optineurin (OPTN) is a multifunctional protein and its mutations are associated with neurodegenerative diseases such as POAG and amyotrophic lateral sclerosis (ALS). We have previously described an E50K mutation-carrying transgenic (E50K^{tg}) mouse that exhibited glaucomatous phenotypes of decreased retinal ganglion cells (RGCs) and surrounding cell death at normal IOP. Further phenotypic analysis of these mice revealed persistent reactive gliosis and E50K mutant protein deposits in the outer plexiform layer (OPL). Over-expression of E50K in HEK293 cells indicated accumulation of insoluble OPTN in the endoplasmic reticulum (ER). This phenomenon was consistent with the results seen in neurons derived from induced pluripotent stem cells (iPSCs) from E50K mutation-carrying NTG patients. The E50K mutant strongly interacted with TANK-binding kinase 1 (TBK1), which prohibited the proper oligomerization and solubility of OPTN, both of which are important for OPTN intracellular transition. Treatment with a TBK1 inhibitor, BX795, abrogated the aberrant insolubility of the E50K mutant. Here, we delineated the intracellular dynamics of the endogenous E50K mutant protein for the first time and demonstrated how this mutation causes OPTN insolubility, in association with TBK1, to evoke POAG.

INTRODUCTION

Glaucoma is one of the world's leading cause of adult-onset blindness that causes optic nerve degeneration characterized by progressive and irreversible loss of retinal ganglion cells (RGCs) and retinal nerve fiber layer defects accompanied by the corresponding visual field damage (1). Open-angle glaucoma, the most prevalent subtype among various glaucomas, is further subdivided into two major types according to intraocular pressure (IOP). In the high-IOP type or primary open-angle glaucoma (POAG), elevated IOP due to disturbance of aqueous humor outflow in the trabecular meshwork or Schlemm's canal mechanically damages RGCs (2). In the normal-IOP type or normal-tension glaucoma (NTG), IOP elevation does not necessarily cause glaucoma, but some IOP-independent factors are thought to be involved (2). According to a population-based glaucoma survey conducted in Japan, NTG is the most prevalent subtype of glaucoma in the country (3, 4). This epidemiological study in Japan reported that the subjects' average IOP was ~15 mmHg and the POAG prevalence was almost equivalent in groups with IOP higher or lower than the average IOP (4). We have investigated the onset mechanism of the latter glaucoma subset, with lower IOP than average, as NTG. Interestingly enough, IOP-unrelated genetic mutations have been found recently in NTG (5, 6) and the Optineurin (OPTN) E50K mutation was the first one identified in familial NTG (7).

OPTN, a scaffold protein with various biological functions, has a few coiled-coil domains and a ubiquitin-binding domain

*To whom correspondence should be addressed at: Division of Molecular and Cellular Biology, National Institute of Sensory Organs, National Hospital Organization Tokyo Medical Center, 2-5-1 Higashigaoka, Meguro-ku, Tokyo 152-8902, Japan. Tel/Fax: +81 334111026; Email: iwatatakeshi@kankakuki.go.jp

at C-terminal. It associates with membrane trafficking proteins Myosin VI and Rab 8 to form Golgi ribbons and is involved in exocytosis (8, 9). And thus E50K mutation yields several phenotypes, such as fragmentation of Golgi apparatus (10), transport failure (8, 11) or apoptotic cell death (12, 13).

OPTN also participates in innate immunity response by regulating NF-kB activation and autophagy in anti-infection processes (14, 15) and via its interaction with some other proteins (16). Among the several OPTN mutations described in the original report, the role of a glutamic acid-to-lysine conversion at amino acid 50 (E50K) in NTG is well accepted worldwide (17–19). A family with a history of NTG was previously identified with the E50K mutation, and in affected members of this family, visual failure starts at about the age of 30 years (Supplementary Material, Fig, S1) and progresses to glaucoma without elevation of IOP until vision is entirely lost at about the age of 70 years (19). Recently, Maruyama *et al.* (20) identified three additional mutations in *OPTN*, a deletion in exon 5, a nonsense mutation (Q398X) and a missense mutation (E478G) that was associated with amyotrophic lateral sclerosis (ALS). Among these three mutations, the former two were recessive mutations and the latter E478G mutation was a dominant mutation, like E50K. The authors further showed the attenuation of the inhibitory effect of NF-kB activation by OPTN carrying the E478G mutation, but that the inhibitory function remained intact with the E50K mutation. Though the underlying causes of OPTN mutation-driven changes are different in POAG and ALS, it is still intriguing that OPTN plays crucial roles in neural homeostasis.

All these results suggest that the E50K mutant expression restricts retinal neural cell survival and is thus involved in the progression of POAG. The underlying molecular mechanism of how the glaucoma phenotype is evoked by a single amino acid replacement in OPTN is still unknown.

In this study, we further characterized the effects of the E50K mutation in OPTN in E50K transgenic ($E50K^{-tg}$) mice and explored the endogenous OPTN dynamics in neural cells differentiated from induced pluripotent stem cells (iPSCs) derived from NTG patients with the genetic mutation corresponding to E50K. At the molecular level, abnormal insolubility of the endogenous E50K OPTN mutant was demonstrated in this study for the first time. This insolubility was simultaneously attributed to the formation of a distinct protein complex, and to disabled oligomerization of OPTN, associated with an enhanced E50K–tank-binding kinase (TBK)1 interaction. The abnormal insolubility of the E50K mutant was rescued by treatment with a TBK1-specific inhibitor.

RESULTS

OPTN E50K transgenic mice exhibit profound gliosis in the retina

In our previous report, we showed that $E50K^{-tg}$ mice exhibited phenotypes, such as a decreased number of RGCs and progressive diminution of retinal thickness without elevation of IOP (19). Immunohistochemistry of the flat-mount retinas of $E50K^{-tg}$ mice showed persistent glial fibrillary acidic protein (GFAP)-positive dot-staining between astrocytes, compared with the staining pattern in retinas of wild-type mice (Fig. 1A and B). Evaluation of the pathological condition in age-matched wild-type and mutant mice by pathologists blinded to the sample source indicated significantly increased gliosis in the $E50K^{-tg}$ mice, compared with the wild-type mice (Fig. 1C). GFAP-positive Müller cells are known as one of the hallmarks for retinal neurodegenerative conditions, including glaucoma (21), which can be simulated by various retinal insults such as the optic nerve axonal damage, laser ablation and intravitreal injection of kainic acid (22–24). From the morphological analysis of the cells that appeared in the vertically incised retinal surface (Fig. 1D, dashed line), the GFAP-positive dots shown in the flat-mount specimen were concluded to be Müller cells, from their peculiar spindle shape (Fig. 1D, arrowheads). Reactive gliosis has been reported to be associated with retinal physical insults; thus, this phenotype in $E50K^{-tg}$ mice in the absence of physical insults was of particular interest. Therefore, in addition to the reactive gliosis in the retinas of $E50K^{-tg}$ mice, the retinal vessels were examined by *z*-axis confocal laser microscopy after tail vein injection of red fluorescent dye-conjugated isolectin. The confocal microscopy images revealed a number of gliosis scars embracing leakage of isolectin from vessels (Supplementary Material, Fig. S2A). These findings suggest that the retinas of $E50K^{-tg}$ mice are under continuous stress and are structurally vulnerable.

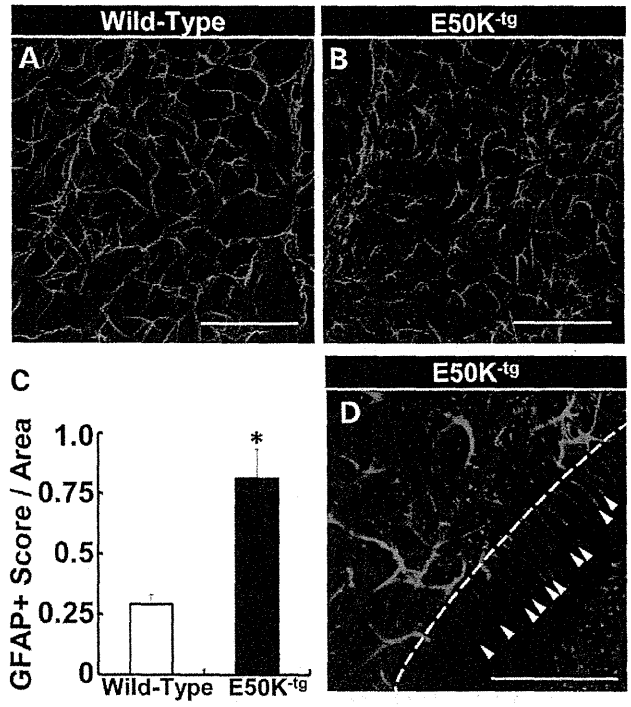

Figure 1. Persistent reactive gliosis in E50K-transgenic ($E50K^{-tg}$) mouse retinas. Representative retinal flat-mount immunohistochemistry images of anti-GFAP in (A) wild-type and (B) $E50K^{-tg}$ mice. Scale bar 200 mm. Flat-mount specimens were analyzed (blinded evaluation) for gliosis assessment. The scores of GFAP-positive gliosis area/retinal area are plotted (data are mean + SD; four fields of micrographs were chosen randomly and analyzed from one specimen, n 4, $^*P$, 0.05). (D) The appearance of GFAP-positive Müller cells in $E50K^{-tg}$ mice. The dashed line indicates the border of the retinal luminal surface and the incised surface of the retina; arrowheads indicate the feet of GFAP-positive astrocytes. Scale bar 100 mm. Some of the gliosis harbors the retinal vessel leakage (Supplementary Material, Fig. S1A).

OPTN E50K protein accumulates in the outer plexiform layer of the retinas of E50K^{-tg} mice

Considering the previous report of the deposit-like pathology in motor neurons in the ALS-associated OPTN E478G mutation (20), we also investigated the localization of the OPTN E50K protein in the retinas of E50K^{-tg} mice by immunohistochemistry. Negative control slides, treated with rabbit IgG cocktail alone, did not exhibit significant signals (Fig. 2A and B), while the retinas of E50K^{-tg} mice exhibited positive staining for OPTN in the outer plexiform layer (OPL) and the inner nuclear layer (INL), as small dot-like deposits (Fig. 2D and F, arrows). The retinas of wild-type littermates did not exhibit such a pattern (Fig. 2C and E). We designed this transgenic mouse with N-terminally HA-tagged OPTN protein, which would enable us to confirm whether the deposits include E50K mutant protein. HA-tagged E50K was mainly detected in the OPL of the retinas in E50K^{-tg} mice, which was consistent with the immunostaining results with the anti-OPTN antibody (Supplementary Material, Fig. S3D, arrows). Positive signals were not detected for OPTN in control slides in the retinas of wild-type mice and in those treated with the IgG alone (Supplementary Material, Fig. S3A–C). Thus, OPTN deposits in the retinas of E50K^{-tg} mice were caused exclusively from the expression of the E50K mutant. These pathology findings point to the capacity of the E50K mutant protein to aggregate.

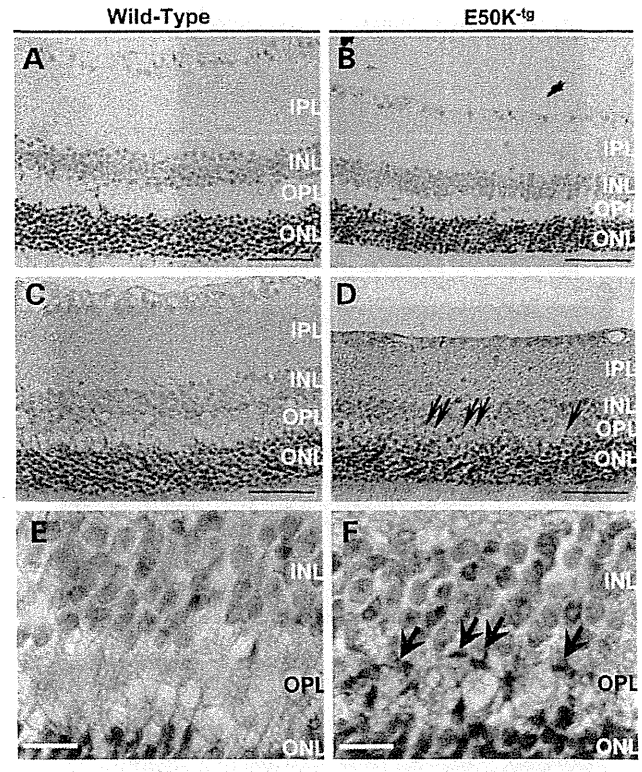

Figure 2. E50K mutant protein deposits in the retinas of E50K^{-tg} mice. (A) Rabbit IgG negative control for the immunohistochemistry analysis of the retina of a wild-type mouse. (B) Rabbit IgG negative control for the immunohistochemistry analysis of the retina of an E50K^{-tg} mouse. Both negative control slides showed minimum background staining. (C) Anti-OPTN immunohistochemistry of the wild-type mouse retina. Moderate OPTN signals were detected in luminal to inner layers of the retina. (D) Anti-OPTN immunohistochemistry of the E50K^{-tg} mouse. In addition to the moderate OPTN signals similar to that in the wild-type mouse retina, some strong deposit-like signals from INL to OPL were detected (indicated with arrows). Scale bars 50 mm. High magnification micrograph of the retina of (E) wild-type and (F) E50K^{-tg} mice. Arrows indicate the OPTN deposit-like signals. Scale bars 10 mm. The OPTN signals consists of, at least to some extent, the E50K^{-tg} transgene product, from the results of immunohistochemistry analysis with an anti-HA antibody (Supplementary Material, Fig. S2D). INL, inner nuclear layer; OPL, outer plexiform layer; ONL, outer nuclear layer.

Examination of induced neural cells from NTG patient-derived iPSCs indicates disturbed OPTN transition from ER to Golgi and Golgi body constriction

To clarify the cause of E50K mutant protein deposits in the retinas of E50K^{-tg} mice, we first examined the intracellular localization of wild-type OPTN and the E50K mutant by transfecting vectors encoding the two proteins fused with enhanced green fluorescent protein (EGFP) (^{EGFP}-OPTN and ^{EGFP}-E50K, respectively) into HEK 293 cells. ^{EGFP}-OPTN could be seen as small puncta widely distributed intracellularly, while ^{EGFP}-E50K was seen as larger puncta accumulated in the perinuclear region, and the Golgi body in the E50K-expressing cells was fragmented (Supplementary Material, Fig. S4B, arrowheads) as previously reported (10, 20). Since Golgi body formation and its membrane trafficking are associated with the endoplasmic reticulum (ER) (25, 26), ER structure was also examined using an ER detection kit (ER-ID, Enzo). Again, the wild-type OPTN was observed as small puncta dispersed within the cytosol (Fig. 3A), while the larger vesicles of the E50K mutant were accumulated in the perinuclear region surrounded by the ER membrane (Fig. 3B, arrows). To elucidate the intracellular localization of endogenous OPTN, we generated induced pluripotent stem cells (iPSCs) from peripheral blood mononuclear cells isolated from NTG patients with the mutation corresponding to E50K and examined OPTN localization in these cells. The pluripotency of iPSCs was confirmed by immunostaining with antibodies specific for Oct3 and Nanog, pluripotency markers (Supplementary Material, Fig. S5A). Neural induction was conducted as previously reported (27, 28) and neuronal differentiation was confirmed by staining with an antibody specific for Tuj1, a neuronal marker (Supplementary Material, Fig. S5B). iPSC-derived neural cells from NTG patients with the mutation corresponding to E50K were immunostained for OPTN and GM130, as a Golgi body marker, along with ER staining. In the iPSCs with wild-type OPTN, derived from a non-glaucoma subject, OPTN-associated vesicles were dispersed within the cells from ER to Golgi networks, in a pattern identical to that in HEK293 cells over-expressing wild-type OPTN (Fig. 3C). However, in the iPSCs from the NTG patient with the mutation corresponding to E50K, the number of OPTN-associated vesicles was decreased, compared with that in the control iPSCs, with dense aggregation in perinuclear regions and shrinkage of the ER/Golgi body (Fig. 3D). Upon microscopic examination under higher magnification, we found that wild-type OPTN frequently localized on the tips of Golgi ribbons (Fig. 3E), while the E50K OPTN mutant in iPSCs from NTG patients accumulated in the ER and Golgi body (Fig. 3F). Co-localization of wild-type OPTN and the Golgi body was

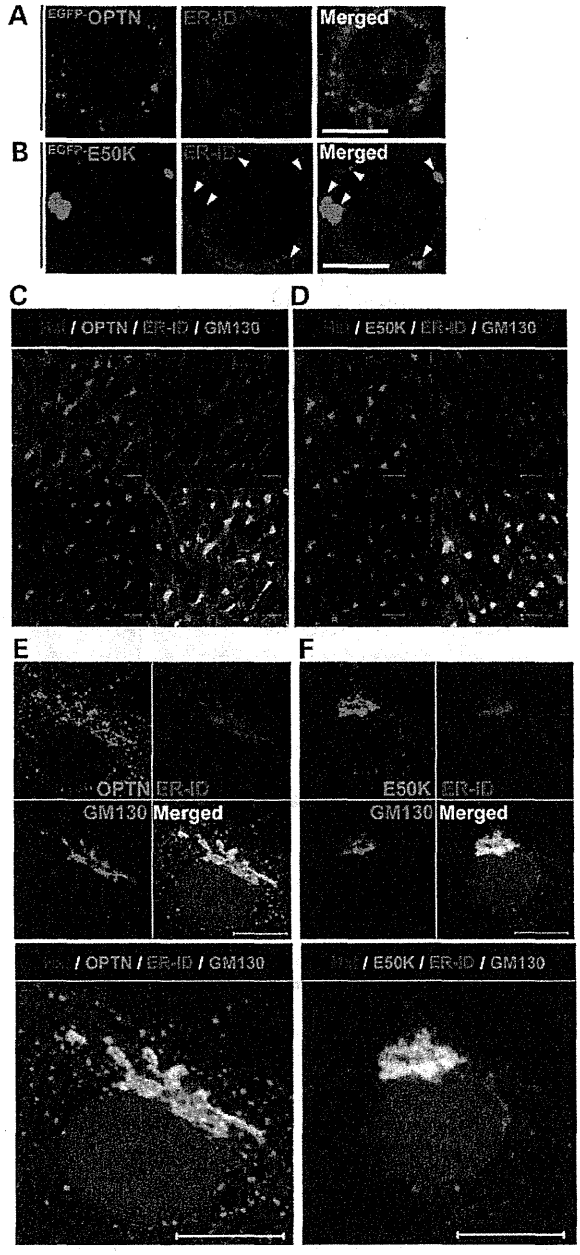

Figure 3. Distinct intracellular localization of wild-type OPTN and the E50K mutant. Intracellular localization of OPTN and E50K in over-expression studies. (A) ^{EGFP}-OPTN (green) and ER (red) localization 1 day after transfection. (B) ^{EGFP}-E50K mutant (green) and ER (red) localization 1 day after transfection. Both micrographs are shown with nuclear counter-staining with Hoechst 33342 (blue). Arrowheads indicate the E50K accumulation in the ER. Scale bars 10 μm. iPSCs were established from iPSCs without the E50K mutation, derived from non-glaucoma subjects, as a control and with the E50K mutation, derived from glaucoma patients for endogenous analyses. Ten days after neural induction, OPTN (green), ER (red) and Golgi (magenta) co-localization were analyzed by immunocytochemistry. (C) Endogenous OPTN localization in neural control cells or (D) E50K glaucoma patient-derived neural cells. OPTN signals exhibited an accumulated pattern in cells with the E50K mutation. Higher magnification of endogenous OPTN signals in (E) control cells and (F) cells with the E50K mutation. In control cells, OPTN signals (green vesicles) were localized on the tips of ribbon Golgi body, while in the cells with the E50K mutation, the number of OPTN signals was decreased and largely accumulated within the ER and to a shrunken Golgi body (shown by the white signal in merged micrographs, respectively). All scale bars 10 μm.

frequently observed (Supplementary Material, Fig. S4A, arrow), but such a co-localization was scarce for the E50K mutant (Supplementary Material, Fig. S4B). These results indicate that the expression of the E50K mutant affects OPTN transition from ER to Golgi body prior to Golgi shrinkage/fragmentation.

Insolubility of OPTN in iPSCs and iPSC-derived neural cells from NTG patients with the mutation corresponding to E50K

While performing the over-expression experiments, we noticed that the protein amount of over-expressed E50K was decreased to half that of wild-type OPTN in HEK293T cells. A similar result has been previously reported in dermal fibroblasts from the E50K mutation-carrying patients (29). Since there was no significant difference in the mRNA levels in both groups (Supplementary Material, Fig. S6A), we speculated that E50K is more susceptible to intracellular degradation. Our previous studies have shown that OPTN is degraded by proteasomal and lysosomal pathways (30). Therefore, we first treated cells with MG132, a proteasomal inhibitor, and bafilomycin, a lysosomal inhibitor, along with cycloheximide, a protein synthesis inhibitor, to compare the amount of protein degradation. The levels of over-expressed OPTN in cells treated only with cycloheximide were lower, while co-treatment with MG132 or bafilomycin restored the OPTN protein levels, as previously reported (Supplementary Material, Fig. S7A, OPTN lanes). However, over-expressed E50K mutant protein was not restored, unlike over-expressed wild-type OPTN, upon treatment of cells with inhibitors (Supplementary Material, Fig. S7A, E50K lanes). These results indicate that there was no association between the lower levels of the E50K mutant and intracellular degradation of OPTN. We predicted that E50K might be expressed at levels comparable to the wild-type protein, but was probably insoluble and was being precipitated with the insoluble pellet (Ppt.) fraction of the cell lysate after routine cell-lysate collection. Although an equivalent amount of calnexin, a Ppt. marker, was detected in the Ppt. fraction of both wild-type- and E50K-expressing HEK293 cells, ~2- to 5-fold higher amounts of E50K protein, compared with the wild-type OPTN, was detected in the Ppt. fraction (Fig. 4A and B). The insolubilized E50K increased in an E50K expression-dependent manner (Fig. 4C). To elucidate the reason for this altered solubility of E50K mutant protein, we utilized the aforementioned iPSCs and examined the OPTN protein levels by western blotting. Although the OPTN expression was moderate in undifferentiated iPSCs, OPTN was detected in the Sup. fraction of control iPSC lysates (Fig. 4D, control 1–4), while OPTN was detected in the Ppt. fraction of iPSCs from NTG patients with the mutation corresponding to E50K (Fig. 4D, E50K 1–6). OPTN expression was significantly increased after neural induction (Fig. 4E Sup. lanes). The iPSC-derived neural cells recapitulated these results, i.e. abundant OPTN in the Ppt. fraction in E50K mutation-carrying NTG patient-derived cells (Fig. 4E, Ppt. lanes). These findings indicate that regardless of the expression levels, the E50K mutant protein exhibits higher intracellular insolubility.

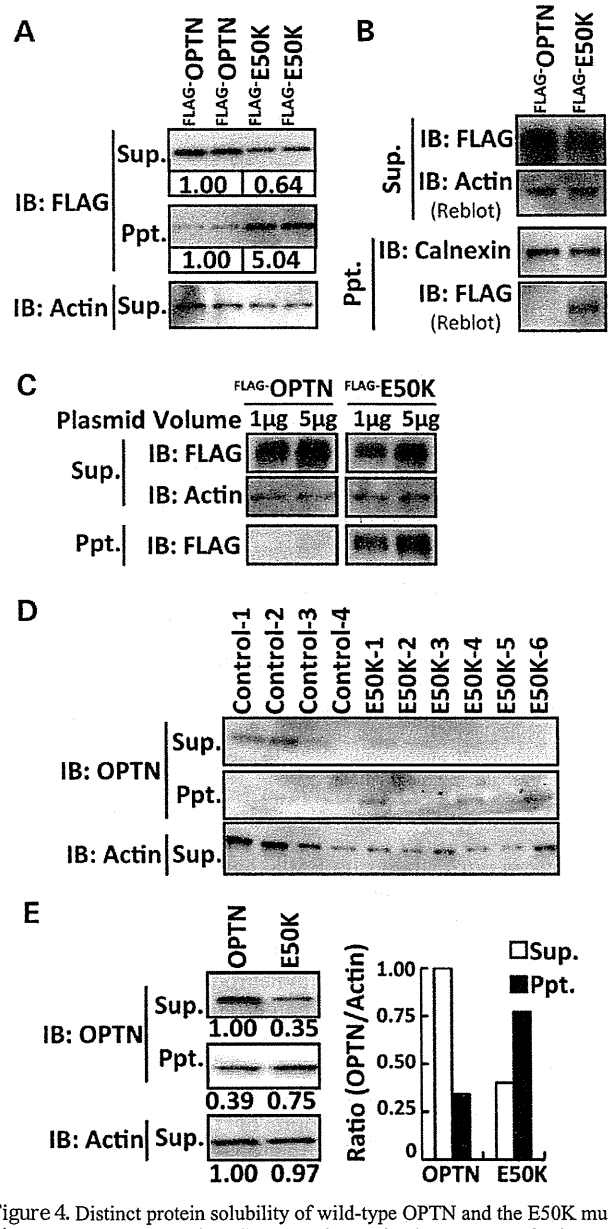

Figure 4. Distinct protein solubility of wild-type OPTN and the E50K mutant. (A) Wild-type OPTN and E50K expression under the same transfection condition. There were no differences in mRNA expressions under these transfection conditions (Supplementary Material, Fig. S4A). The 'Missing' E50K mutant protein was detected in the precipitated fraction (Ppt.), after supernatant (Sup.) collection. Semi-quantitative western blotting analysis was performed using Chemidoc (BioRad) with imaging software and the results are shown under each band. Approximately 2-fold reduction of E50K mutant protein in the Sup. fraction and 2- to 5-fold induction in the Ppt. fraction were observed. (B) Although calnexin, an ER membrane marker, is detected in both the Ppt. fraction of wild-type OPTN-expressing and E50K mutant-expressing cells, only the E50K mutant is detected in the Ppt. fraction. (C) The E50K mutant in the Ppt. fraction was increased in an E50K expression-dependent manner. (D) Endogenous expression and higher hydrophobicity of OPTN in iPSCs with the E50K mutation. Endogenous OPTN is also detected in the Ppt. fraction in iPSCs from E50K mutation-carrying NTG patients. (E) Abundant endogenous expression and higher hydrophobicity of OPTN in iPSC-derived neural cells 10 days after induction from E50K mutation-carrying NTG patients. Semi-quantitative western blotting analysis by Chemidoc with imaging software was performed and the results are shown under each band. The OPTN amounts in each fraction were normalized to the actin amount and then plotted. Sup., supernatant fraction; Ppt., precipitated fraction.

The enhanced affinity of TBK1 to the E50K mutant protein affects the proper oligomerization and solubility of OPTN

To elucidate the factors that affect the solubility of OPTN, we first examined the native state of wild-type OPTN and the E50K mutant. FLAG-tagged OPTN was expressed in cells and lysates were routinely prepared without detergent and separated by native-polyacrylamide gel electrophoresis (PAGE). Western blotting analysis after native-PAGE indicated more E50K-protein complexes compared with those formed by wild-type OPTN (Fig. 5A). The complexes were immunoprecipitated (IP) using an anti-FLAG antibody and then separated by SDS–PAGE, which revealed distinct binding partners of OPTN and E50K (Fig. 5B, OPTN, white arrowheads; E50K, black arrowheads). We identified each binding partner by liquid chromatography–tandem mass spectrometry (LC–MS/MS). The OPTN partner was identified as OPTN itself, indicating tight oligomerization, while the E50K protein partner was identified as TBK1, which has been previously shown to interact with OPTN by a yeast two-hybrid screening (31). Each candidate interacting partner was further confirmed by IP and western blotting (Fig. 5C and D). Intriguingly, E50K exhibited enhanced affinity to TBK1, while its self-oligomerization was largely decreased (Fig. 5C, arrowhead). Oligomerized OPTN bands clearly seen in wild-type OPTN were restored by treatment with intracellular degradation inhibitors (Supplementary Material, Fig. S7A, left panel, Oligomer lanes), indicating the importance of OPTN oligomerization in intracellular traffic and intracellular degradation. In contrast, these intracellular inhibitors had no effect on the diminished oligomerization of the E50K mutant (Supplementary Material, Fig. S7A right panel, Oligomer lanes). Treatment with a specific inhibitor treatment for TBK1, BX975 (32), was used to examine the relevance of TBK1 binding and the abnormal insolubility of the E50K mutant. BX795 treatment had no effects on the trace amounts of either wild-type OPTN (Supplementary Material, Fig. S7B) or calnexin in the Ppt. fraction (Fig. 5E); on the other hand, the amount of the insolubilized E50K mutant in the Ppt. fraction was drastically decreased by treatment with BX795 in a concentration-dependent manner. Prolonged BX795 treatment was able to restore the E50K mutant protein to the Sup. fraction (Fig. 5F). These findings indicate that the enhanced affinity of E50K for TBK1 is one of the initial pathogenic events that trigger the intracellular insolubility of OPTN leading to improper OPTN transition from the ER to the Golgi body.

DISCUSSION

The OPTN E50K mutation is the only mutation currently affirmed as causative for NTG, and therefore, it is a clinically relevant mutation for elucidating the mechanism of disease onset at a molecular level (4). Although the E50K mutation is a rare event in familial POAG, the pathology is usually progressive, leading to full blindness even under strict IOP control (Supplementary Material, Fig. S1) (17). Previous reports on E50K mutant phenotypes were focused mainly on *in vitro* models using over-expression studies. Though our initial report on the phenotypic analyses of E50K^{-tg} mice was informative (19), there is a strong necessity for further establishment of the model for OPTN and its target molecules in the endogenous

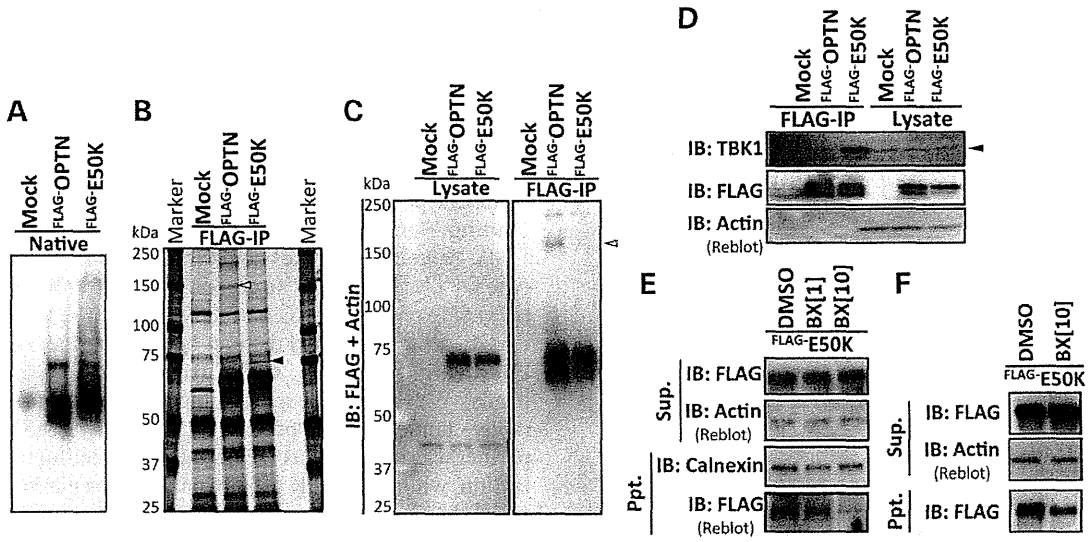

Figure 5. Constitutive interaction of the E50K mutant protein and TBK1 evokes the aberrant solubility of OPTN. (A) Native-PAGE of mock-transfected controls, wild-type OPTN-transfected cells and E50K-transfected cells revealed the distinct protein complex formation. (B) Silver-staining of immunoprecipitates of mock-transfected controls, wild-type OPTN-transfected cells and E50K-transfected cells using an antibody specific for the FLAG-tag. The relevant bands, wild-type OPTN-specific binding molecule (white arrowhead) and E50K mutant-specific binding molecule (black arrowhead), were detected and further analyzed with LC–MS/MS. (C) Oligomerization of OPTN. The band indicated with white arrowhead in (B) turned out OPTN itself, i.e. wild-type OPTN is able to oligomerize, while E50K mutant protein largely lacks this oligomerization ability. (D) E50K mutant and TBK1 interaction. The band indicated with black arrowhead in (B) turned out TBK1 and E50K mutant protein exhibited higher affinity to TBK1 protein than wild-type OPTN. (E) The treatment with BX795, a TBK1 inhibitor, decreases the aberrant precipitation of E50K mutant protein in the Ppt. fraction in a concentration-dependent manner. Dimethylsulfoxide (DMSO) was used as the vehicle control and BX [1], BX [10] indicates the BX795 treatment concentrations of 1 μg/ml and 10 μg/ml, respectively, for 3 h. (F) Longer treatment with BX795 (6 h with 10 μg/ml) suppressed aberrant precipitation of E50K mutant protein in the Ppt. fraction and simultaneously restored E50K to the soluble fraction.

context to understand the exact molecular functions of OPTN and its mutations in glaucoma. In addition to the previously identified glaucomatous phenotypes, such as RGC loss, E50K^{-tg} mice also exhibit prominent retinal reactive gliosis with GFAP-positive Müller cells. It has been reported that GFAP-positive Müller cells can be experimentally induced in animal models mimicking glaucomatous phenotypes through various retinal insults, such as axonal damage, intravitreal injection and laser ablation (22–24). Thus, the persistent gliosis and inner layer cell death in E50K^{-tg} mice, without elevation of IOP, were of great interest, and this suggests that increased IOP is not the sole cause for POAG. The deposit-like E50K mutant protein seen in the INL of the retinas of E50K^{-tg} mice was encouraging, because similar abnormal protein inclusions are frequently found in clinical specimens of neurodegenerative tissues, including ALS (20, 33). Why E50K expression, which occurs throughout the body, only affects retinal homeostasis remains unknown. OPTN is also endogenously expressed in many other types of cells, like fibroblasts (7). In addition, most of the other cells expressing OPTN are proliferative and replaced usually within a few months, whereas the neural cells are usually non-proliferative and long-lived. We surmise that this is why the accumulation of E50K over time is critical in the pathogenesis of neurodegenerative diseases, including NTG. Though the E50K^{-tg} mice exhibit some representative neurodegenerative disease phenotypes, further investigation of the E50K accumulation in the endogenous context over time *in vivo* in the retina is needed, preferable in retinal specimens from E50K mutation-carrying NTG patient or from a mouse model, such as a site-specific knock-in mouse model.

Previous *in vitro* studies on E50K have shown large vesicle formation and Golgi fragmentation (10, 20), while there are no reports of endogenous E50K localization and behavior, especially in patient neuronal cells. In general, data pertaining to OPTN in clinical samples of patients with neurodegenerative diseases, including the retinal disease, is scarce. The iPSC technology is one solution to overcome this longstanding limitation by indirectly generating the desired target cells from iPSCs derived from patients with genetically driven neurodegenerative diseases (34). With this first report of the establishment of E50K-glaucoma iPSCs and their neuronal induction, molecular and cellular characterization of POAG onset can now be studied in the endogenous context. iPSC-derived neural cells from E50K mutation-carrying patients revealed for the first time that OPTN accumulated at the constricted Golgi body. In our current experiments, unlike the results of the E50K over-expression studies, Golgi was constricted but not fragmented. This discrepancy should be carefully examined to elucidate whether fragmentation of Golgi body is an endogenous phenotype or just an artifact induced by the over-expression. In any case, excess accumulation of E50K triggers Golgi body deformation and further deteriorates intracellular traffic, and eventually leads to cell death. It is well known that OPTN has a role in secretory vesicle transport and that E50K expression decreases the release of the neurotrophic factor NT3 (9, 35). Furthermore, prostaglandin E2 (PGE2) release via exocytosis is also decreased by E50K expression (Supplementary Material, Fig. S1B). These results indicate that due to the intracellular transport failure in cells expressing the E50K mutant, the paracrine activity for cellular protection and blood flow within the retina would also be attenuated.

Retinal vessel vulnerability in E50K^{-tg} mice is explained by these indirect extracellular E50K effects.

This study demonstrated that the E50K mutant is insoluble and is associated with the hydrophobic precipitate in lysates, compared with the wild-type OPTN, in iPSCs and iPSC-derived neural cells. Abnormal protein deposits, as shown in the retinas of the E50K^{-tg} mice, and protein hydrophobicity are frequently reported in neurodegenerative diseases (36–38). Recent reports in yeast models also supported the distinct hydrophobicities of wild-type OPTN and the E50K mutant (39). Although the prediction of isoelectric points (Compute pI/Mw, ExPASy) of wild-type OPTN and E50K do not differ (OPTN 5.21, E50K 5.26), their intracellular protein complex formation is considerably different. The amino acid characteristic of hydrophobic glutamate (E) against hydrophilic lysine (K) suggests that the E50K mutation is a possible charge swap mutation. E50K is located adjacent to the coiled-coil domain, which is a domain implicated in the interaction between OPTN and TBK1 (31, 15). The hydrophobicity of the E50K mutant was closely related with its enhanced interaction with TBK1, a well-known infection-responsive molecule. TBK1 induces macroautophagy by interacting with wild-type OPTN only under conditions of infection, and mediates crosstalk between innate immune response and autophagy (15). Additionally, the copy number variation of *TBK1* was associated with NTG onset (5, 6). The duplication of genes on chromosome 12q14 with familial POAG suggested that an extra copy of the *TBK1* gene and its copy number variation were responsible for NTG (40). More recently, NTG-related TBK1 mutations were also reported (41). Thus it is now well established that both *OPTN* and *TBK1* missense mutations are related with NTG onset. The abnormal physical protein interaction with TBK1 is responsible for the major cause of NTG in relation to the OPTN-E50K mutation. Together with the clinical facts, it has been reported that TBK1 has an important role in innate immunity pathways, and phosphorylated the ER-resident adaptor protein stimulator of IFN genes (STING) to enable IFN production (42, 43). Complexes of these molecules may be involved with the failure of the E50K OPTN protein to transition from ER to Golgi. Although TBK1 contributes to infection-related immunological responses, it also seems to contribute to the intracellular clearance of unnecessary components, such as by autophagy (15). Many other ophthalmic diseases, like macular diseases, are associated with abnormal protein metabolism (44); thus, the crosstalk of OPTN and TBK1 in the maintenance of intracellular clearance in retinal cells is likely to play a significant role in not only glaucomatous but also various other retinal diseases. Even though the exact function of TBK1 and the mechanism of the OPTN-TBK1 crosstalk in retinal homeostasis needs to be elucidated, compounds that abrogate the interaction between the E50K mutant and TBK1 are likely to be beneficial in the treatment of NTG patients.

Our current results pinpoint the molecular basis and concepts of NTG onset in E50K mutation-carrying patients and suggest that the RGC loss, the hallmark of glaucoma, is rather a terminal consequence of the sequential events, i.e. altered affinity of the E50K mutant inhibits self-oligomerization, leading to increased hydrophobicity, which affects downstream functions of OPTN, and eventually leads to cell death. Chronic and excessive accumulation of the E50K mutant protein recapitulated the partial neurodegenerative pathology, including reactive gliosis, vulnerability of retinal vessels and increased apoptotic cell death.

RGC loss is a hallmark of glaucoma; however, the results of this study showed that this phenomenon in E50K-NTG model is at the terminal stage of sequential abnormal events in the retina. In-depth characterization of the mutant protein in a physiologically relevant context and the proper choice/availability of a suitable animal model will help to elucidate and explore therapeutics for personalized treatment of glaucoma in the future.

MATERIALS AND METHODS

Antibodies and biochemical analysis

All the antibodies for biochemical studies were purchased from the following companies: anti-OPTN antibody (Cayman); anti-TBK1 antibody (Cell Signaling Technology); anti-FLAG (Sigma); anti-HA (Roche) and anti-Actin (Millipore). The TBK1 inhibitor, BX795, and cycloheximide were purchased from Calbiochem. Mini-PROTEAN TGX Gel and Transblot turbo system (BioRad) were used for native and SDS–PAGE western blotting according to the manufacturer's instructions. Quantitative western blotting was performed with ChemiDoc XRS+ with the Image lab software package (Biorad).

Animal experiments, preparation of retinal at-mounts for staining and immunohistochemistry

All animal experiments were carried out in accordance with the Guide for the Care and Use of Laboratory Animals (National Institutes of Health) and the Association for Research in Vision and Ophthalmology Statement for the Use of Animals in Vision Research and approved by the Tokyo Medical Center Experimental Animal Committee. The OPTN mutant E50K^{-tg} mouse used in this study has been described previously (19). Twenty-two to 24-month-old male E50K^{-tg} mice (n 4) and their littermates (n 4) were sacrificed for the assessment of retinal gliosis. Both eyes were dissected and immunostained in flat-mounts as previously described (19). Briefly, dissected eyes were fixed in 2% paraformaldehyde and permeabilized with 0.1% Triton-phosphate-buffered saline (PBS). Nonspecific binding was prevented by blocking with DAKO's serum-free blocking buffer, and all specimens were incubated with Alex488-conjugated anti-GFAP antibody (Millipore) for 48C, over two nights. After radial dissection, retinas were mounted in DAKO's fluorescent mounting medium. A total of 16 retinal specimens, with four micrographs per one retinal specimen, were imaged by LSM700 confocal fluorescence microscopy (Zeiss) using a blinded method. Image analysis was conducted using the ZEN software (Zeiss) and the GFAP-positive area per retinal area was scored. The anti-OPTN (Cayman) and anti-HA (COVANCE) antibodies were used under heated antigen-retrieval conditions. Endogenous peroxidase was quenched by 3% H_2O_2 in MeOH. After primary antibody reaction for 48C overnight, simple rabbit IgG-horse radish peroxidase (HRP) stain and mouse IgG-HRP stain for mouse tissue (Nichirei) were used as secondary HRP-conjugated polymers. After developing with 3,3′-diaminobenzidine (DAB) substrate, specimens were counter-stained with Gill's hematoxylin.

Light microscopy was performed with an Eclipse 600 microscope (Nikon).

Cell culture, transfection and immunocytochemistry

HEK293T cells were cultured in Dulbecco's modified Eagle medium (DMEM), supplemented with 10% heat-inactivated FBS. The TransIT-PRO Transfection Kit (Mirus) was used according to the manufacturer's instructions. HEK293T cells were transfected with pAC-^{GFP}, pAC-^{GFP}-OPTN and pAC-^{GFP}-E50K to assess the intracellular localization of tagged OPTN. The ER-ID Red assay kit (Enzo) was used for endoplasmic reticulum staining. Anti-GM130 and Alexa633-conjugated anti-mouse IgG antibodies were used for Golgi immunostaining. The following constructs were used for over-expression studies: pEF-BOS-^{FLAG} (45), pEF-BOS-^{FLAG}-Optineurin and pEF-BOS-^{FLAG}-E50K.

Generation of iPSC and induction of differentiation to neural cells

Human E50K mutation-carrying iPSCs and the corresponding control iPSCs were established by Sendai-viral (DNAVEC) infection as previously reported (46) from circulating T-cells in the peripheral blood of human familial glaucoma patients with fully informed consent. All procedures were approved by the Ethics Committee of National Hospital Organization Tokyo Medical Center. For maintaining the pluripotency, iPSCs were cultured in bovine fibroblast growth factor (bFGF)-containing iPSC media on Matrigel-coated culture dishes. Oct3 and Nanog were used as pluripotency markers and Tuj1 was used as the neuronal marker. Neural cell induction was performed via embryoid body formation as described previously (27, 28), utilizing the Neuron differentiation Kit (R&D Systems) in accordance with the manufacturer's procedures.

Identi cation of E50K-binding proteins by LC MS/MS

Samples for LC–MS/MS analysis were prepared by preparing lysates from HEK293T cells over-expressing FLAG-tagged OPTN from pEF-BOS-^{FLAG}, pEF-BOS-^{FLAG}-Optineurin or pEF-BOS-^{FLAG}-E50K. Each lysate sample was immunoprecipitated with M2-FLAG-Agarose (Sigma) for 2 h at 48C. The immunoprecipitated beads were washed with lysis buffer five times and then eluted with 2 M urea. The eluates were electrophoresed on 7.5% SDS–PAGE gels and the gels were silver-stained with the Silver Quest Kit (Invitrogen). The band of interest was processed for in-gel digestion for further LC–MS/MS analysis. Samples were analyzed with LCQ-DECA XP (Thermo Scientific). The obtained binding candidates and their interaction with OPTN/E50K were confirmed by immunoprecipitation and western blotting.

SUPPLEMENTARY MATERIAL

Supplementary Material is available at HMG online.

FUNDING

This work was supported by grants to T.I. by the Japanese Ministry of Health, Labour and Welfare (10103254), National Hospital Organization of Japan and the Japan Society for the Promotion of Science (09005752 to T.I., 24791885 to Y.M.). The pEF-BOS vector was a kind gift from Dr Seisuke Hattori in Kitasato University.

AUTHOR CONTRIBUTIONS

Y.M. and T.I designed the study; Y.M., D.I., H.K., Z.-L.C., H.K., performed the experiments; K.K., T.Y., T.S., S.Y., K.F. contributed new reagents/techniques; Y.M. and T.I. analyzed the data; Y.M. and T.I. wrote the paper.

REFERENCES

1. Quigley, H.A. and Broman, A.T. (2006) The number of people with glaucoma worldwide in 2010 and 2020. *Br. J. Ophthalmol.*, 90, 262–267.
2. Quigley, H.A. (2011) Glaucoma. *Lancet*, 377, 1367–1377.
3. Suzuki, Y., Iwase, A., Araie, M., Yamamoto, T., Abe, H., Shirato, S., Kuwayama, Y., Mishima, H.K., Shimizu, H., Tomita, G. *et al.* (2006) Risk factors for open-angle glaucoma in a Japanese population: the Tajimi Study. *Ophthalmology*, 113, 1613–1617.
4. Iwase, A., Suzuki, Y., Araie, M., Yamamoto, T., Abe, H., Shirato, S., Kuwayama, Y., Mishima, H.K., Shimizu, H., Tomita, G. *et al.* (2004) The prevalence of primary open-angle glaucoma in Japanese: the Tajimi Study. *Ophthalmology*, 111, 1641–1648.
5. Fingert, J.H., Robin, A.L., Stone, J.L., Roos, B.R., Davis, L.K., Scheetz, T.E., Bennett, S.R., Wassink, T.H., Kwon, Y.H., Alward, W.L. *et al.* (2011) Copy number variations on chromosome 12q14 in patients with normal tension glaucoma. *Hum. Mol. Genet.*, 20, 2482–2494.
6. Kawase, K., Allingham, R.R., Meguro, A., Mizuki, N., Roos, B., Solivan-Timpe, F.M., Robin, A.L., Ritch, R. and Fingert, J.H. (2012) Confirmation of TBK1 duplication in normal tension glaucoma. *Exp. Eye Res.*, 96, 178–180.
7. Rezaie, T., Child, A., Hitchings, R., Brice, G., Miller, L., Coca-Prados, M., Heon, E., Krupin, T., Ritch, R., Kreutzer, D. *et al.* (2002) Adult-onset primary open-angle glaucoma caused by mutations in optineurin. *Science*, 295, 1077–1079.
8. Sahlender, D.A., Roberts, R.C., Arden, S.D., Spudich, G., Taylor, M.J., Luzio, J.P., Kendrick-Jones, J. and Buss, F. (2005) Optineurin links myosin VI to the Golgi complex and is involved in Golgi organization and exocytosis. *J. Cell Biol.*, 169, 285–295.
9. Bond, L.M., Peden, A.A., Kendrick-Jones, J., Sellers, J.R. and Buss, F. (2011) Myosin VI and its binding partner optineurin are involved in secretory vesicle fusion at the plasma membrane. *Mol. Biol. Cell*, 22, 54–65.
10. Park, B.C., Shen, X., Samaraweera, M. and Yue, B.Y. (2006) Studies of optineurin, a glaucoma gene: Golgi fragmentation and cell death from overexpression of wild-type and mutant optineurin in two ocular cell types. *Am. J. Pathol.*, 169, 1976–1989.
11. Nagabhushana, A., Chalasani, M.L., Jain, N., Radha, V., Rangaraj, N., Balasubramanian, D. and Swarup, G. (2010) Regulation of endocytic trafficking of transferrin receptor by optineurin and its impairment by a glaucoma-associated mutant. *BMC Cell Biol.*, 11, 4.
12. Chalasani, M.L., Radha, V., Gupta, V., Agarwal, N., Balasubramanian, D. and Swarup, G. (2007) A glaucoma-associated mutant of optineurin selectively induces death of retinal ganglion cells which is inhibited by antioxidants. *Invest. Ophthalmol. Vis. Sci.*, 48, 1607–1614.
13. Meng, Q., Lv, J., Ge, H., Zhang, L., Xue, F., Zhu, Y. and Liu, P. (2012) Overexpressed mutant optineurin(E50K) induces retinal ganglion cells apoptosis via the mitochondrial pathway. *Mol. Biol. Rep.*, 39, 5867–5873.
14. Gleason, C.E., Ordureau, A., Gourlay, R., Arthur, J.S. and Cohen, P. (2011) Polyubiquitin binding to optineurin is required for optimal activation of TANK-binding kinase 1 and production of interferon beta. *J. Biol. Chem.*, 286, 35663–35674.
15. Wild, P., Farhan, H., McEwan, D.G., Wagner, S., Rogov, V.V., Brady, N.R., Richter, B., Korac, J., Waidmann, O., Choudhary, C. *et al.* (2011)

Phosphorylation of the autophagy receptor optineurin restricts Salmonella growth. *Science*, 333, 228–233.
16. Ying, H. and Yue, B.Y. (2012) Cellular and molecular biology of optineurin. *Int. Rev. Cell. Mol. Biol.*, 294, 223–258.
17. Aung, T., Rezaie, T., Okada, K., Viswanathan, A.C., Child, A.H., Brice, G., Bhattacharya, S.S., Lehmann, O.J., Sarfarazi, M. and Hitchings, R.A. (2005) Clinical features and course of patients with glaucoma with the E50K mutation in the optineurin gene. *Invest. Ophthalmol. Vis. Sci.*, 46, 2816–2822.
18. Hauser, M.A., Sena, D.F., Flor, J., Walter, J., Auguste, J., Larocque-Abramson, K., Graham, F., Delbono, E., Haines, J.L., Pericak-Vance, M.A. *et al.* (2006) Distribution of optineurin sequence variations in an ethnically diverse population of low-tension glaucoma patients from the United States. *J. Glaucoma*, 15, 358–363.
19. Chi, Z.L., Akahori, M., Obazawa, M., Minami, M., Noda, T., Nakaya, N., Tomarev, S., Kawase, K., Yamamoto, T., Noda, S. *et al.* (2010) Overexpression of optineurin E50K disrupts Rab8 interaction and leads to a progressive retinal degeneration in mice. *Hum. Mol. Genet.*, 19, 2606–2615.
20. Maruyama, H., Morino, H., Ito, H., Izumi, Y., Kato, H., Watanabe, Y., Kinoshita, Y., Kamada, M., Nodera, H., Suzuki, H. *et al.* (2010) Mutations of optineurin in amyotrophic lateral sclerosis. *Nature*, 465, 223–226.
21. Ganesh, B.S. and Chintala, S.K. (2011) Inhibition of reactive gliosis attenuates excitotoxicity-mediated death of retinal ganglion cells. *PLoS One*, 6, e18305.
22. Wurm, A., Iandiev, I., Uhlmann, S., Wiedemann, P., Reichenbach, A., Bringmann, A. and Pannicke, T. (2011) Effects of ischemia-reperfusion on physiological properties of Muller glial cells in the porcine retina. *Invest. Ophthalmol. Vis. Sci.*, 52, 3360–3367.
23. Giani, A., Thanos, A., Roh, M.I., Connolly, E., Trichonas, G., Kim, I., Gragoudas, E., Vavvas, D. and Miller, J.W. (2011) In vivo evaluation of laser-induced choroidal neovascularization using spectral-domain optical coherence tomography. *Invest. Ophthalmol. Vis. Sci.*, 52, 3880–3887.
24. Ueda, K., Nakahara, T., Hoshino, M., Mori, A., Sakamoto, K. and Ishii, K. (2010) Retinal blood vessels are damaged in a rat model of NMDA-induced retinal degeneration. *Neurosci. Lett.*, 485, 55–59.
25. Lasiecka, Z.M. and Winckler, B. (2011) Mechanisms of polarized membrane trafficking in neurons – focusing in on endosomes. *Mol. Cell. Neurosci.*, 48, 278–287.
26. Farhan, H., Freissmuth, M. and Sitte, H.H. (2006) Oligomerization of neurotransmitter transporters: a ticket from the endoplasmic reticulum to the plasma membrane. *Handb. Exp. Pharmacol.*, 175, 233–249.
27. Tsuji, O., Miura, K., Okada, Y., Fujiyoshi, K., Mukaino, M., Nagoshi, N., Kitamura, K., Kumagai, G., Nishino, M., Tomisato, S. *et al.* (2010) Therapeutic potential of appropriately evaluated safe-induced pluripotent stem cells for spinal cord injury. *Proc. Natl Acad. Sci. USA*, 107, 12704–12709.
28. Tucker, B.A., Scheetz, T.E., Mullins, R.F., DeLuca, A.P., Hoffmann, J.M., Johnston, R.M., Jacobson, S.G., Sheffield, V.C. and Stone, E.M. (2011) Exome sequencing and analysis of induced pluripotent stem cells identify the cilia-related gene male germ cell-associated kinase (MAK) as a cause of retinitis pigmentosa. *Proc. Natl Acad. Sci. USA*, 108, E569–576.
29. Sarfarazi, M. and Rezaie, T. (2003) Optineurin in primary open angle glaucoma. *Ophthalmol. Clin. North Am.*, 16, 529–541.
30. Shen, X., Ying, H., Qiu, Y., Park, J.S., Shyam, R., Chi, Z.L., Iwata, T. and Yue, B.Y. (2011) Processing of optineurin in neuronal cells. *J. Biol. Chem.*, 286, 3618–3629.
31. Morton, S., Hesson, L., Peggie, M. and Cohen, P. (2008) Enhanced binding of TBK1 by an optineurin mutant that causes a familial form of primary open angle glaucoma. *FEBS Lett.*, 582, 997–1002.
32. Clark, K., Plater, L., Peggie, M. and Cohen, P. (2009) Use of the pharmacological inhibitor BX795 to study the regulation and physiological roles of TBK1 and IkappaB kinase epsilon: a distinct upstream kinase mediates Ser-172 phosphorylation and activation. *J. Biol. Chem.*, 284, 14136–14146.
33. Ito, H., Nakamura, M., Komure, O., Ayaki, T., Wate, R., Maruyama, H., Nakamura, Y., Fujita, K., Kaneko, S., Okamoto, Y. *et al.* (2011) Clinicopathologic study on an ALS family with a heterozygous E478G optineurin mutation. *Acta Neuropathol.*, 122, 223–229.
34. Imaizumi, Y., Okada, Y., Akamatsu, W., Koike, M., Kuzumaki, N., Hayakawa, H., Nihira, T., Kobayashi, T., Ohyama, M., Sato, S. *et al.* (2012) Mitochondrial dysfunction associated with increased oxidative stress and alpha-synuclein accumulation in PARK2 iPSC-derived neurons and postmortem brain tissue. *Mol. Brain*, 5, 35.
35. Sippl, C., Bosserhoff, A.K., Fischer, D. and Tamm, E.R. (2011) Depletion of optineurin in RGC-5 cells derived from retinal neurons causes apoptosis and reduces the secretion of neurotrophins. *Exp. Eye Res.*, 93, 669–680.
36. Nukina, N., Kosik, K.S. and Selkoe, D.J. (1987) Recognition of Alzheimer paired helical filaments by monoclonal neurofilament antibodies is due to crossreaction with tau protein. *Proc. Natl Acad. Sci. USA*, 84, 3415–3419.
37. Hoffner, G., Kahlem, P. and Djian, P. (2002) Perinuclear localization of huntingtin as a consequence of its binding to microtubules through an interaction with beta-tubulin: relevance to Huntington's disease. *J. Cell Sci.*, 115, 941–948.
38. LaVoie, M.J., Ostaszewski, B.L., Weihofen, A., Schlossmacher, M.G. and Selkoe, D.J. (2005) Dopamine covalently modifies and functionally inactivates parkin. *Nat. Med.*, 11, 1214–1221.
39. Kryndushkin, D., Ihrke, G., Piermartiri, T.C. and Shewmaker, F. (2012) A yeast model of optineurin proteinopathy reveals a unique aggregation pattern associated with cellular toxicity. *Mol. Microbiol.*, 86, 1531–1547.
40. Fingert, J.H., Darbro, B.W., Qian, Q., Van Rheeden, R., Miller, K., Riker, M., Solivan-Timpe, F., Roos, B.R., Robin, A.L. and Mullins, R.F. (2013) TBK1 and flanking genes in human retina. *Ophthalmic Genet.*, doi:10.3109/13816810.2013.768674.
41. Seo, S., Solivan-Timpe, F., Roos, B.R., Robin, A.L., Stone, E.M., Kwon, Y.H., Alward, W.L. and Fingert, J.H. (2013) Identification of proteins that interact with TANK binding kinase 1 and testing for mutations associated with glaucoma. *Curr. Eye Res.*, 38, 310–315.
42. Saitoh, T., Fujita, N., Hayashi, T., Takahara, K., Satoh, T., Lee, H., Matsunaga, K., Kageyama, S., Omori, H., Noda, T. *et al.* (2009) Atg9a controls dsDNA-driven dynamic translocation of STING and the innate immune response. *Proc. Natl Acad. Sci. USA*, 106, 20842–20846.
43. Tanaka, Y. and Chen, Z.J. (2012) STING specifies IRF3 phosphorylation by TBK1 in the cytosolic DNA signaling pathway. *Sci. Signal.*, 5, ra20.
44. Shaw, P.X., Zhang, L., Zhang, M., Du, H., Zhao, L., Lee, C., Grob, S., Lim, S.L., Hughes, G., Lee, J. *et al.* (2012) Complement factor H genotypes impact risk of age-related macular degeneration by interaction with oxidized phospholipids. *Proc. Natl Acad. Sci. USA*, 109, 13757–13762.
45. Mizushima, S. and Nagata, S. (1990) pEF-BOS, a powerful mammalian expression vector. *Nucleic Acids Res.*, 18, 5322.
46. Seki, T., Yuasa, S., Oda, M., Egashira, T., Yae, K., Kusumoto, D., Nakata, H., Tohyama, S., Hashimoto, H., Kodaira, M. *et al.* (2010) Generation of induced pluripotent stem cells from human terminally differentiated circulating T cells. *Cell Stem Cell*, 7, 11–14.

Characterizing the Phenotype and Genotype of a Family With Occult Macular Dystrophy

Connie J. Chen, MD; Hendrik P. N. Scholl, MD, MA; David G. Birch, PhD; Takeshi Iwata, PhD; Neil R. Miller, MD; Morton F. Goldberg, MD

Objective: To characterize the phenotype of a white patient with occult macular dystrophy (OMD) and her clinically unaffected family members and to determine whether similar mutations were present in the *RP1L1* gene in this family. Occult macular dystrophy is a rare macular dystrophy with central cone dysfunction hidden behind a normal fundus appearance that has been attributed to a mutation in the retinitis pigmentosa 1–like 1 (*RP1L1*) gene in 4 Japanese families.

Methods: In this observational cross-sectional study of 1 white family with OMD, patients meeting the clinical criteria for OMD and their family members were evaluated by use of multifocal electroretinography, the Farnsworth D-15 color vision test, automated perimetry, spectral-domain optical coherence tomography (SD-OCT), fundus autofluorescence, and fundus photography. Fluorescein angiography was performed only on the proband. Members of this family were screened for genetic mutations in the *RP1L1* gene.

Results: In the family studied, the clinically affected proband was noted to have loss of the foveal outer segments and absence of bowing of the inner segment/outer segment junction on SD-OCT scans. In addition, 1 clinically unaffected family member also demonstrated loss of the foveal photoreceptor outer segments and, therefore, decreased bowing of the inner segment/outer segment junction on SD-OCT scans. The fundus autofluorescence images of the eyes of the proband and her family members were normal. Although mutations in the *RP1L1* gene have been identified in sporadic and autosomal dominant OMD pedigrees, no mutations in the *RP1L1* gene were found in any of the participants.

Conclusions: Loss of the outer segments of foveal photoreceptors can be detected and quantified by use of SD-OCT in patients with OMD. Similar findings are present in some clinically unaffected family members and may represent subclinical manifestations of the disease. Although mutations in the *RP1L1* gene have been described in several Japanese families with OMD, there were no such mutations in this white family of European descent, which suggests that inherited OMD is a genetically heterogeneous disorder.

Arch Ophthalmol. 2012;130(12):1554-1559

Author Affiliations: Wilmer Eye Institute, Baltimore, Maryland (Drs Chen, Scholl, Miller, and Goldberg); National Institute of Sensory Organs, Tokyo, Japan (Dr Iwata); and the Retina Foundation of the Southwest and University of Texas Southwestern Medical Center, Dallas, Texas (Dr Birch).

In 1989, Miyake et al[1] first described the autosomal dominant inheritance of a hereditary macular dystrophy without visible fundus abnormalities. In all patients, focal macular electroretinography gave significantly abnormal results, making this test the gold standard for diagnosis. Several years later, after patients with similar findings were described in other parts of the world,[2] the condition was renamed occult macular dystrophy (OMD).[3] To date, there have been about 71 reported cases of OMD that often have been confused initially with more common ocular disorders, such as normal-tension glaucoma, retrobulbar optic neuritis, amblyopia, and even nonorganic visual loss.[1-10]

Recently, spectral-domain optical coherence tomographic (SD-OCT) studies of patients with OMD have identified more subtle abnormalities in the retina of affected individuals, including disruptions in the inner segment/outer segment (IS/OS) junction of the photoreceptor layer, the absence of the normal "bowing effect" seen in normal IS/OS junctions, and the loss of cone outer segment tips.[4-6,8] To the best of our knowledge, no imaging studies of clinically unaffected family members have been reported.

Akahori et al[11] recently identified mutations in the retinitis pigmentosa 1–like 1 (*RP1L1*) gene in 4 Japanese families with OMD and suggested that these mutations were responsible for autosomal dominantly inherited OMD. To date, no genetic studies have been performed on white families of European descent with OMD. We assessed both clinically affected and

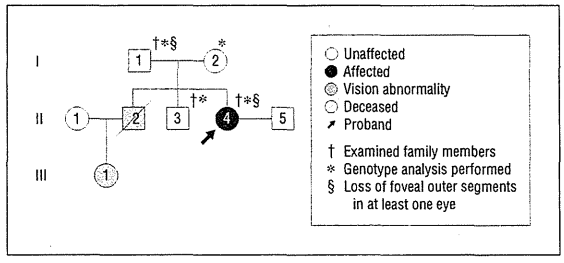

Figure 1. Family pedigree of a white family with occult macular dystrophy (OMD). A white patient with OMD and her clinically unaffected family members were tested to determine whether similar mutations were present in the *RP1L1* gene.

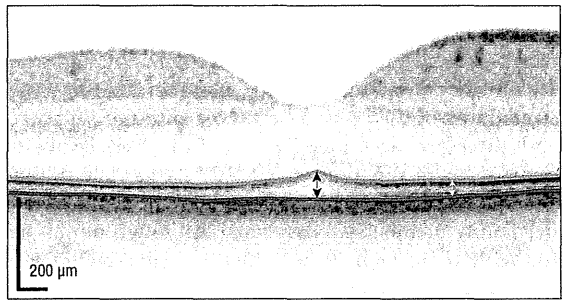

Figure 2. Effective foveal outer segment length. Segmentation analysis is shown for an unrelated normal patient. The green segmentation line marks the inner boundary, and the red segmentation line marks the outer boundary of the outer segment layer. The black double arrow shows the foveal outer segment length measured by computer-assisted manual segmentation. The white double arrow shows the measurement of the outer segment length 3° nasal from the foveal center. The effective outer segment length is the outer segment length 3° nasal to the fovea (white double arrow) subtracted from the foveal outer segment length (black double arrow).

unaffected family members in 1 white pedigree with OMD clinically, electrophysiologically, and with SD-OCT, and we also screened these individuals for genetic mutations in the *RP1L1* gene.

METHODS

The protocol and consent forms were approved by the Johns Hopkins Hospital institutional review board. Families with OMD were recruited from the Wilmer Eye Institute in Baltimore, Maryland. For all recruited participants, written informed consent was obtained.

INCLUSION AND EXCLUSION CRITERIA

Patients who met the following clinical criteria for OMD were included in our study: normal fundus appearance, normal fluorescein angiogram, and abnormal macular function suggested by an abnormal multifocal electroretinogram (mfERG). Patients were judged to have an abnormal mfERG of clinical significance if the amplitude of the central element (ring 1, subtending <2.4°) was below the fifth percentile of normative values or if the implicit times exceeded the 95th percentile of normative values. All available immediate family members of affected patients were recruited to participate in our study (participants indicated by cross bars and asterisks in **Figure 1**). Families were excluded if the proband had an abnormal fundus appearance (eg, retinal flecks, bull's-eye maculopathy, or macular scarring) or an abnormal full-field ERG.

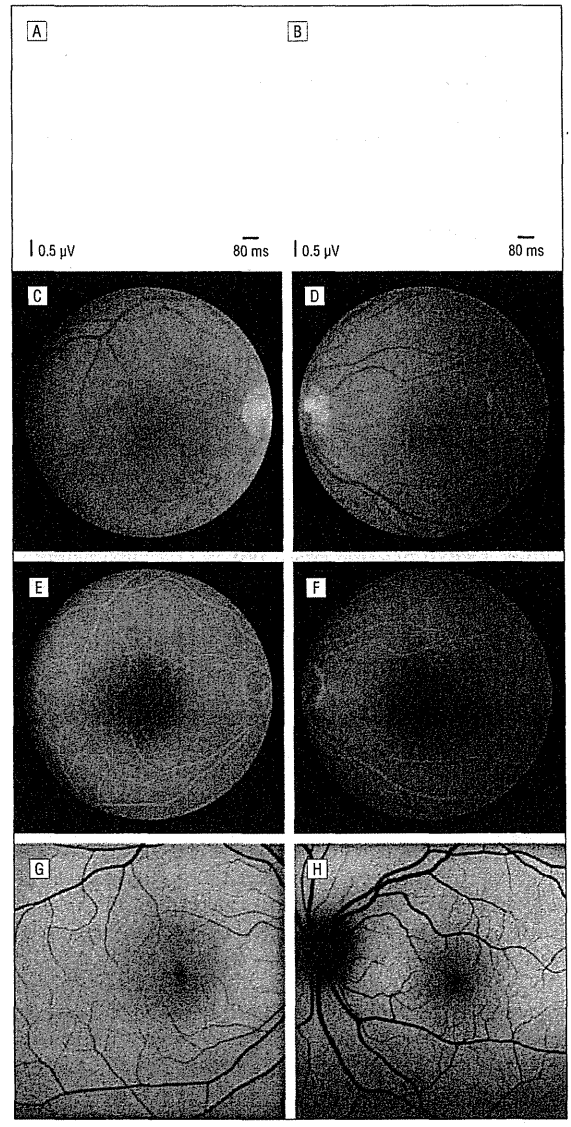

Figure 3. Multifocal electroretinograms of the proband (II-4) revealing decreased central amplitudes in the right eye (A) and the left eye (B). The proband's right eye (C) and left eye (D) have a normal fundus appearance. Fluorescein angiography was performed on the right eye (E) and the left eye (F), and the angiograms were normal. Fundus autofluorescence images are normal for both the right eye (G) and the left eye (H).

CLINICAL ASSESSMENT

During their initial study visit, participants underwent Snellen best-corrected visual acuity testing and Farnsworth D-15 color vision testing, automated perimetry (Humphrey 10-2 threshold test, SITA Standard) was performed, and color fundus images and fundus autofluorescence images were obtained. Fluorescein angiography was performed for probands only.

ELECTROPHYSIOLOGIC AND OCT ASSESSMENT

The mfERGs were recorded one eye at a time with the Visual Evoked Response Imaging System Version 5.2 (EDI) using a Burian-Allen contact lens ERG electrode in accordance with In-

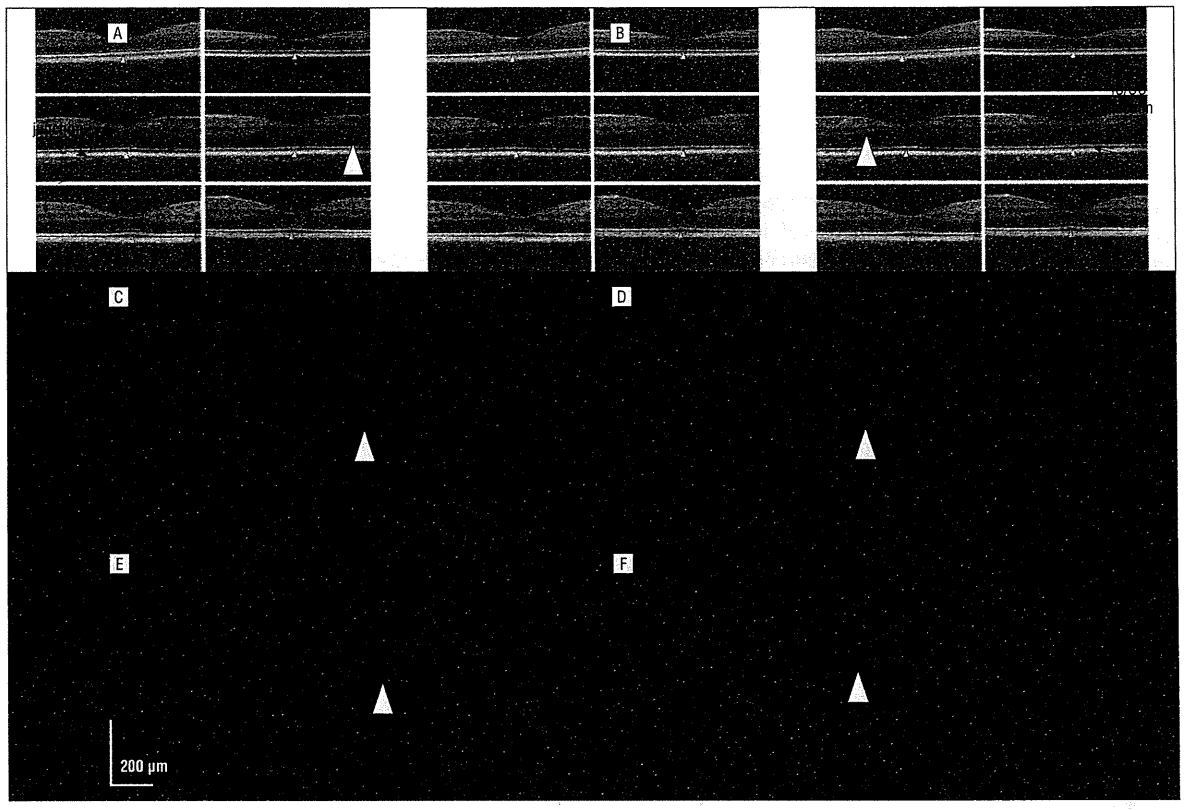

Figure 4. Spectral-domain optical coherence tomographic images of family members. There is marked loss of the outer segments (arrowheads) with absence of bowing of the inner segment/outer segment (IS/OS) junction in the right eye (A) and left eye (B) of the proband (II-4). For the clinically unaffected father (I-1), bowing of the IS/OS junction is absent in the right eye (C) and the left eye (D) but is preserved in the clinically unaffected brother's (II-3) right eye (E) and left eye (F). RPE indicates retinal pigment epithelium.

ternational Society for Clinical Electrophysiology of Vision standards. Both eyes were dilated with cyclopentolate hydrochloride, 1%, and phenylephrine hydrochloride, 2.5%. The visual stimuli consisted of a 103 hexagonal array. The luminance of each hexagon was independently modulated according to a binary m-sequence at 75 Hz. The data were compared against a database of 48 normal eyes for 6 distinct rings of hexagons.

Spectralis OCT (Heidelberg Engineering) imaging was also performed for all participants. Horizontal line scans through the fovea, captured by use of SD-OCT, were segmented using computer-assisted manual segmentation in a masked fashion based on a previously published protocol.[12] Participants with other unrelated foveal pathology (eg, foveal drusen or disciform scar) identified during imaging were excluded from segmentation analysis. The horizontal line scan with the most appreciable bowing of the IS/OS junction was selected after manually reviewing all horizontal scans to ensure that the correct line scan through the fovea was chosen, even with eccentric fixation. To quantify the "bowing effect" seen in normal healthy foveal architecture,[13,14] we subtracted the length of the outer segments at a point 3° nasal to the fovea (see the white double arrow in **Figure 2**) from the foveal outer segment (see the black double arrow in Figure 2) for each eye. We defined the measurement for each individual eye, which we termed the *effective foveal outer segment length* (eFOSL). The eFOSL is the outer segment length 3° nasal to the fovea (white double arrow) subtracted from the foveal outer segment length (black double arrow).

The same computer-assisted manual segmentation analysis was performed on a set of 62 normal eyes for which SD-OCT images were available to create a normative database for comparison (obtained at the Retina Foundation of the Southwest, Dallas, Texas). The eFOSL was obtained for all normal eyes in the database using horizontal line scans.

GENETIC TESTING

Genetic testing for the *RP1L1* gene was performed on all available participants (indicated by asterisks in Figure 1) at the National Hospital Organization Tokyo Medical Center at the National Institute of Sensory Organs in Japan, using previously described methods.[11] The DNA from peripheral blood was extracted, and direct sequencing was performed on all the exons and flanking regions of the *RP1L1* gene. We define mutation as amino acid change that is expected to influence protein function. This mutation should segregate within the family and never be detected in the normal population. The study participants were carefully compared against age-matched normal individuals with no visual abnormalities recorded in the database of single-nucleotide polymorphisms maintained by the National Center for Biotechnology Information.

RESULTS

In this family (Figure 1), there was 1 clinically affected proband (II-4) with OMD. The patient described central visual loss beginning at 42 years of age, at which point she was found to have a best-corrected visual acuity of 20/400 in the right eye and 20/30 in the left eye, bilateral central

scotomas, normal results from an ophthalmoscopic examination, and a normal fluorescein angiogram. At that time, she received a diagnosis of normal-tension glaucoma, although no glaucomatous optic nerve cupping was noted. Five years later, her visual acuity in the left eye had decreased further to 20/125. At this time, a mfERG revealed a clinically significant decrease of foveal response amplitudes in both eyes, compatible with OMD (**Figure 3**). Spectral-domain OCT revealed marked loss of the foveal outer segments with a flattening of the normally bowed IS/OS junction (**Figure 4**A and B). Her eFOSL was markedly abnormal, measuring 0 μm in both eyes (**Figure 5**).

The proband's father (I-1) did not have any visual complaints. On clinical examination, his best-corrected visual acuity was 20/25 bilaterally. He had mild cataracts and bilateral extrafoveal nonneovascular age-related macular degeneration. His foveas appeared to be normal. A mfERG revealed a clinically significant reduction in foveal response amplitude in the right eye and a normal foveal response amplitude in the left eye (**Table**). He had delayed ring 1 implicit times in both eyes. Spectral-domain OCT revealed marked loss of the foveal outer segments and decreased bowing of the IS/OS junction bilaterally (Figure 4C and D). The eFOSL was decreased in both eyes, measuring 6 μm in the right eye and 2 μm in the left eye (Figure 5).

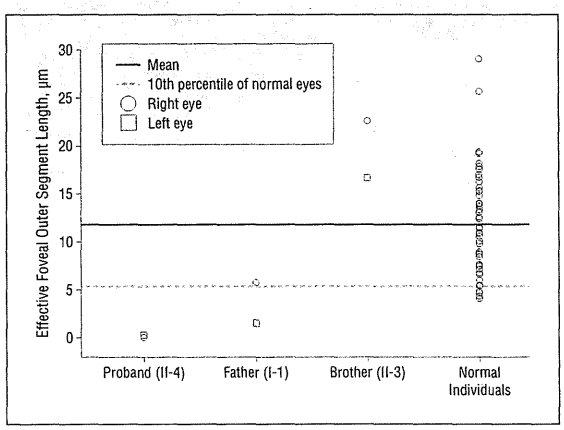

Figure 5. The effective foveal outer segment lengths for the proband (II-4) and 2 family members (I-1 and II-3) shown alongside those of individuals with normal eyes. The dotted line represents the 10th percentile effective foveal outer segment length for normal eyes. The mean effective foveal outer segment length in 62 normal eyes is 12 μm.

One brother (II-2) had been evaluated previously by an ophthalmologist and was presumed to have OMD based on clinical history and clinical examination, but neither multifocal electroretinography nor OCT was ever performed. The patient died of an unrelated health condition during the study period and, therefore, was unavailable for further testing.

Another of the proband's brothers (II-3) denied any visual complaints and had normal results from an ophthalmoscopic examination and normal foveal response amplitudes and normal ring 1 implicit times on a mfERG. In this individual, SD-OCT revealed a normal outer segment length with preserved bowing of the IS/OS junction (Figure 4E and F) and a normal eFOSL of 23 μm in the right eye and 17 μm in the left eye (Figure 5).

The proband's mother (I-2) was unavailable for clinical assessment, multifocal electroretinography, or imaging, but she underwent genetic testing. Fundus autofluorescence images for all 3 tested family members were normal (images not shown except for proband II-4; Figure 3G and H). Sequencing of the exons of the *RP1L1* gene of the proband, mother, father, and one brother (I-1, I-2, II-3, and II-4) revealed no mutations.

COMMENT

For patients with OMD, there is a growing amount of data collected with SD-OCT imaging that can be compared against a normative database. Rangaswamy et al[12] have developed a segmentation technique to measure the outer segment length on SD-OCT; for normal individuals, the outer segment length is increased centrally and decreased in the periphery, creating a central bowing effect of the IS/OS junction, a normal phenomenon in foveal cone specialization.[13,14] Four previous studies[4-6,8] have examined structural abnormalities on SD-OCT images of patients with OMD. These studies[4-6,8] have described abnormalities in the IS/OS junction and decreased bow-

Table. Clinical Characteristics of Proband and Family Members With Occult Macular Dystrophy[a]

Patient No./Sex/Age, y	*RP1L1* Mutation	Eye	BCVA	Amplitude-Reduced mfERG			Increased Latency in Ring 1	Farnsworth D-15 Color Vision Test Result	eFOSL, μm	Fundus Autofluorescence Image
				Ring 1	Ring 2	Ring 3				
I-1/M/73	No	OD	20/25	+	+	+	+	Normal	6	Extrafoveal drusen
		OS	20/25	–	+	+	+	Normal	2	Normal
II-2/F/71	No	OD	NA	NA	NA	NA	NA	NA	NA	NA
		OS	NA	NA	NA	NA	NA	NA	NA	NA
II-3/M/51	No	OD	20/20	–	–	–	+	Normal	23	Normal
		OS	20/20	–	–	–	–	Normal	17	Normal
II-4/F/48	**No**	**OD**	**20/400**	+	+	+	+	–	**0**	**Normal**
		OS	**20/125**	+	+	+	+	–	**0**	**Normal**

Abbreviations: BCVA, best-corrected visual acuity; eFOSL, effective foveal outer segment length; mfERG, multifocal electroretinogram; NA, not available; –, absent; +, present.

[a]Bold indicates affected proband. The central amplitude corresponds to ring 1 in the mfERG, which subtends less than 2.4° from eccentricity.

ing of the IS/OS junction in OMD patients. Park et al[8] examined unilateral or asymmetric cases, and in 3 of 5 cases, SD-OCT revealed morphologic changes in the photoreceptor layers, even in the eyes with normal vision. Park et al[8] suggested that there is a subclinical stage in the better eye that eventually progresses to clinically manifest OMD. In our study, affected OMD eyes did have abnormalities in the photoreceptor outer segments and demonstrated decreased bowing of the IS/OS junction, which, for the first time, we quantified with segmentation analysis and compared against normal eyes. Interestingly, 1 clinically unaffected family member with no visual symptoms (I-1) demonstrated decreased bowing at the IS/OS junction on SD-OCT images. In this case, it is unclear whether the lack of bowing in clinically unaffected patients is simply a variant of normal or is truly a subclinical stage of OMD. Serial examinations over time will reveal whether or not these subclinical phenotypes eventually will progress to clinically manifest OMD in one or both eyes.

Previous studies have not examined clinically unaffected family members with OCT imaging. Abnormalities in the foveal outer segment that were recorded on a mfERG were present in successive generations. These findings suggest that OMD could be an autosomal dominant condition with variable penetrance and/or expressivity. Alternatively, some of the OCT findings and mfERG findings may be spurious (ie, related to foveal drusen or cataract), and, if so, this could suggest that our proband is an isolated case or has a different inheritance pattern (eg, autosomal recessive).

The *RP1L1* gene, which functions in microtubule assembly and stabilization in photoreceptor axonemes,[11] is responsible for at least 7 Japanese families with autosomal dominantly inherited OMD (T. Iwata, PhD, unpublished data, October 31, 2011). The mutations that have previously been reported include the following mutations in *RP1L1*: 2 substitution mutations c.3107T>C (p.Arg45Trp) and c.362C>T (p.Arg45Trp), 1 missense mutation (c.3596 C>G in exon 4), and 1 insertion mutation (c.325insT in exon 2).[11,15,16] To date, no mutations in the *RP1L1* gene have been identified in autosomal recessive pedigrees. In this family, no mutations were identified in the *RP1L1* gene. It appears, therefore, that multiple genes may be responsible for inherited OMD, similar to the genetic heterogeneity seen in retinitis pigmentosa. Alternatively, this family could represent an autosomal recessive form of OMD in which the *RP1L1* gene is not implicated.

Our study also highlights that SD-OCT may be a sensitive tool that can detect structural abnormalities in the photoreceptor layer before functional impairment. Spectral-domain OCT has several advantages over multifocal electroretinography. Images are easier to interpret, are faster to obtain, have high spatial resolution, and have good repeatability. Furthermore, in OMD, in which patients may have dense central scotomas, SD-OCT images of the fovea can still be obtained even in patients with eccentric fixation. In contrast, multifocal electroretinography requires a steady central fixation for accurate interpretation of central amplitudes.

Fundus autofluorescence reveals nonspecific weak hyperautofluorescent changes in the fovea for about 50% of patients with OMD[4]; however, the autofluorescence images obtained from all tested individuals from this family were normal. This suggests that the abnormality does not lie in the retinal pigment epithelium and that fundus autofluorescence may be a useful tool in distinguishing OMD from other retinal dystrophies in which retinal pigment epithelial disease is characteristic.

In conclusion, a thorough examination of symptomatic and asymptomatic patients in this OMD family revealed a previously uncharacterized possible subclinical phenotype. To our knowledge, this is the first time that loss of foveal outer segments is quantitatively characterized in OMD. This loss may be suggestive of, but not pathognomonic for, OMD. Further genetic testing may allow us to understand the causative mutations and inheritance patterns, thus paving the way for development of potential treatments for OMD.

Submitted for Publication: December 13, 2011; final revision received June 17, 2012; accepted June 20, 2012.
Correspondence: Connie J. Chen, MD, Wilmer Eye Institute, 600 N Wolfe St, Woods Bldg 272, Baltimore, MD 21287 (conniejchen@gmail.com).
Conflict of Interest Disclosures: None reported.
Funding/Support: This study was supported by National Institutes of Health core grant P30EY001765 (to Dr Goldberg); by the Wynn-Gund Translational Research Acceleration Program Enhanced Research and Clinical Training Award NNCD-CL-0310.0049-JHU-WG (to Dr Scholl) from the National Neurovision Research Institute and the Foundation Fighting Blindness; by the Macular Degeneration Research Award M2010042 (to Dr Scholl) from the American Health Assistance Foundation; by the unrestricted National Institutes of Health grant EY09076 (to Dr Birch) from the Research to Prevent Blindness Inc; and by the Japanese Ministry of Health, Labour, and Welfare (to Dr Iwata).
Additional Contributions: We thank Yuquan Wen, PhD, for assistance with segmentation and analysis.

REFERENCES

1. Miyake Y, Ichikawa K, Shiose Y, Kawase Y. Hereditary macular dystrophy without visible fundus abnormality. *Am J Ophthalmol.* 1989;108(3):292-299.
2. Brockhurst RJ, Sandberg MA. Optical coherence tomography findings in occult macular dystrophy. *Am J Ophthalmol.* 2007;143(3):516-518.
3. Miyake Y, Horiguchi M, Tomita N, et al. Occult macular dystrophy. *Am J Ophthalmol.* 1996;122(5):644-653.
4. Fujinami K, Tsunoda K, Hanazono G, Shinoda K, Ohde H, Miyake Y. Fundus autofluorescence in autosomal dominant occult macular dystrophy. *Arch Ophthalmol.* 2011;129(5):597-602.
5. Kim YG, Baek SH, Moon SW, Lee HK, Kim US. Analysis of spectral domain optical coherence tomography findings in occult macular dystrophy. *Acta Ophthalmol.* 2011;89(1):e52-e56.
6. Kitaguchi Y, Kusaka S, Yamaguchi T, Mihashi T, Fujikado T. Detection of photoreceptor disruption by adaptive optics fundus imaging and Fourier-domain optical coherence tomography in eyes with occult macular dystrophy. *Clin Ophthalmol.* 2011;5:345-351.
7. Lyons JS. Non-familial occult macular dystrophy. *Doc Ophthalmol.* 2005;111(1):49-56.
8. Park SJ, Woo SJ, Park KH, Hwang JM, Chung H. Morphologic photoreceptor abnormality in occult macular dystrophy on spectral-domain optical coherence tomography. *Invest Ophthalmol Vis Sci.* 2010;51(7):3673-3679.
9. Piao CH, Kondo M, Tanikawa A, Terasaki H, Miyake Y. Multifocal electroretinogram in occult macular dystrophy. *Invest Ophthalmol Vis Sci.* 2000;41(2):513-517.
10. Sisk RA, Berrocal AM, Lam BL. Loss of foveal cone photoreceptor outer seg-

ments in occult macular dystrophy. *Ophthalmic Surg Lasers Imaging.* 2010; 41:1-3. doi:10.3928/15428877-20100215-49.
11. Akahori M, Tsunoda K, Miyake Y, et al. Dominant mutations in RP1L1 are responsible for occult macular dystrophy. *Am J Hum Genet.* 2010;87(3):424-429.
12. Rangaswamy NV, Patel HM, Locke KG, Hood DC, Birch DG. A comparison of visual field sensitivity to photoreceptor thickness in retinitis pigmentosa. *Invest Ophthalmol Vis Sci.* 2010;51(8):4213-4219.
13. Thomas MG, Kumar A, Mohammad S, et al. Structural grading of foveal hypoplasia using spectral-domain optical coherence tomography a predictor of visual acuity? *Ophthalmology.* 2011;118(8):1653-1660.
14. Mohammad S, Gottlob I, Kumar A, et al. The functional significance of foveal abnormalities in albinism measured using spectral-domain optical coherence tomography. *Ophthalmology.* 2011;118(8):1645-1652.
15. Ahn SJ, Woo SJ, Ahn J, et al. *RP1L1* mutation in Korean patients of occult macular dystrophy (OMD). Paper presented at: Annual Meeting of the Association for Vision and Research in Ophthalmology; May 6-10, 2012; Fort Lauderdale, FL.
16. Kameya S, Kabuto T, Takahashi H, et al. Two new mutations in *RP1L1* gene in occult macular dystrophy patients associated with a depolarizing pattern of focal macular ERG. Paper presented at: Association for Vision and Research in Ophthalmology; May 6-10, 2012; Fort Lauderdale, FL.

Correction

Error in PubMed. In the Global Health Editorial titled "Global Burden of Visual Impairment and Blindness" by Bourne et al, published in the May issue of the *Archives* (2012;130[5]:645-647), the link to the collaborators' list was incomplete at the time of publication and posting and is now incorrect in PubMed. The name of one of the members of the GBD Vision Loss Expert Group, Dr Tasanee Braithwaite, should have been cited but was not.

American Journal of Epidemiology

Vol. 176, No. 5
DOI: 10.1093/aje/kws031
Advance Access publication:
August 5, 2012

Human Genome Epidemiology (HuGE) Review

The Association Between Complement Component 2/Complement Factor B Polymorphisms and Age-related Macular Degeneration: A HuGE Review and Meta-Analysis

Ammarin Thakkinstian*, Mark McEvoy, Usha Chakravarthy, Subhabrata Chakrabarti, Gareth J. McKay, Euijung Ryu, Giuliana Silvestri, Inderjeet Kaur, Peter Francis, Takeshi Iwata, Masakazu Akahori, Astrid Arning, Albert O. Edwards, Johanna M. Seddon, and John Attia

* Correspondence to Dr. Ammarin Thakkinstian, Section for Clinical Epidemiology and Biostatistics, Faculty of Medicine, Ramathibodi Hospital, Mahidol University, Bangkok, Thailand (e-mail: ammarin.tha@mahidol.ac.th).

Initially submitted October 20, 2011; accepted for publication January 23, 2012.

The authors performed a systematic review of the association of complement component 2(*C2*)/complement factor B (*CFB*) gene polymorphisms with age-related macular degeneration (AMD). In total, data from 19 studies published between 2006 and 2011 were pooled for 4 polymorphisms: rs9332739 and rs547154 in the *C2* gene and rs4151667 and rs641153 in the *CFB* gene. Data extraction and assessments for risk of bias were independently performed by 2 reviewers. Allele frequencies and allele and genotypic effects were pooled. Heterogeneity and publication bias were explored. Pooled minor allele frequencies for all 4 SNPs were between 4.7% and 9.6% for all polymorphisms, except for an Indian population in which the C allele at rs9332739 was the major allele. For the *C2* polymorphisms, the minor C allele at rs9332739 and the minor T allele at rs547154 carried estimated relative risks (odds ratios) of 0.55 (95% confidence interval (CI): 0.46, 0.65) and 0.47 (95% CI: 0.39, 0.57), respectively. For the *CFB* polymorphisms, the minor A alleles at rs4151667 and rs614153 carried estimated risks of 0.54 (95% CI: 0.45, 0.64) and 0.41 (95% CI: 0.34, 0.51), respectively. These allele effects contributed to an absolute lowering of the risk of all AMD in Caucasian populations by 2.0%–6.0%. This meta-analysis provides a robust estimate of the protective association of *C2/CFB* with AMD.

complement component factor 2; complement factor B; genetic association studies; genetics; genome, human; macular degeneration; meta-analysis; molecular epidemiology

Abbreviations: AMD, age-related macular degeneration; C2, complement component 2; C3, complement component 3; CFB, complement factor B; CFH, complement factor H; HWE, Hardy-Weinberg equilibrium; LD, linkage disequilibrium; OMIM, Online Mendelian Inheritance in Man; OR, odds ratio; PAR, population attributable risk; SE, standard error.

Editor's note: *This article also appears on the website of the Human Genome Epidemiology Network (http://www.cdc.gov/genomics/hugenet/default.htm).*

Age-related macular degeneration (AMD) is one of the leading causes of blindness worldwide (1–4), accounting for half of all new registered cases of blindness (5). With the increase in longevity, the burden of AMD is set to grow, with almost 30% of persons older than 75 years showing early signs of the disease (1, 6, 7). The pathologic hallmark of the disease is drusen, deposits of proteins and lipids, in the retinal pigment epithelium; these deposits, along with pigmentary irregularities, constitute early AMD. Progression to late AMD involves geographic atrophy, in which there is loss of retinal pigment epithelium and photoreceptors and/or neovascularization.

Genome-wide association studies have had considerable success in identifying genetic contributions to complex disorders. The first success in ocular diseases came in 2005,